JOURNAL OF GEOPHYSICAL RESEARCH, VOL. 113, B09202, doi:10.1029/2007JB005444, 2008

Micromechanical modeling of the viscoplastic behavior of olivine

O. Castelnau,[1,2] D. K. Blackman,[1] R. A. Lebensohn,[3] and P. Ponte Castañeda[4]

Received 17 October 2007; revised 11 March 2008; accepted 2 April 2008; published 5 September 2008.

[1] Efforts to couple mantle flow models with rheological theories of mineral deformation typically ignore the effect of texture development on flow evolution. The fact that there are only three easy slip systems for dislocation glide in olivine crystals leads to strong mechanical interactions between the grains as the deformation proceeds, and subsequent development of large viscoplastic anisotropy in polycrystals exhibiting pronounced Lattice Preferred Orientations. Using full-field simulations for creep in dry polycrystalline olivine at high temperature and low pressure, it is shown that very large stress and strain rate intragranular heterogeneities can build up with deformation, which increase dramatically with the strength of the hard slip system (included for the purpose of enabling general deformations). Compared with earlier nonlinear extensions of the Self-Consistent mean-field theory to simulate polycrystal deformation, the ''Second-Order'' method is the only one capable of accurately describing the effect of intraphase stress heterogeneities on the macroscopic flow stress, as well as on the local stress- and strain rate fluctuations in the material. In particular, this approach correctly predicts that olivine polycrystals can deform with only four independent slip systems. The resistance of the fourth system (or accommodation mechanism), which is likely provided by dislocation climb or grain boundary processes as has been observed experimentally, may essentially determine the flow stress of olivine polycrystals. We further show that the ''tangent'' model, which had been used extensively in prior geophysical studies of the mantle, departs significantly from the full-field reference solutions.

Citation: Castelnau, O., D. K. Blackman, R. A. Lebensohn, and P. Ponte Castañeda (2008), Micromechanical modeling of the viscoplastic behavior of olivine, *J. Geophys. Res.*, *113*, B09202, doi:10.1029/2007JB005444.

1. Introduction

[2] The Earth upper mantle is known to exhibit elastic anisotropy, which is commonly attributed to the presence of Lattice Preferred Orientations (LPO; acronyms used in this paper are listed in Table 1). Such anisotropy is revealed in recordings of seismic waves that travel through the mantle with speeds that depend on propagation direction. The development of LPO is due to the plastic deformation of mantle minerals. Peridotite polycrystalline aggregates respond by dislocation creep to forces associated with large-scale convective flow. Both olivine and pyroxene exhibit an orthorhombic crystal structure that has only a few slip systems available for dislocation creep, which can lead to very high viscoplastic anisotropy at the grain scale. Thus upper mantle regions with strong seismic anisotropy (i.e., pronounced LPO) may also exhibit large viscoplastic anisotropy which would manifest itself as large differences between flow stresses in shear and extension (leading to viscosities that can vary typically by one or two orders of magnitude depending on the direction of prescribed plastic strain). Anisotropy may possibly have a large influence on the flow in some regions of the mantle [*Christensen*, 1987; *Kocks et al.*, 1998], as was also shown for the flow of ice in ice sheets [*Mangeney et al.*, 1997], but the topic has received little attention [*Blackman*, 2007].

[3] In this study, the impact of LPO on mantle rheological behavior is assessed through numerical investigation of the viscoplastic behavior of olivine $(Mg, Fe)_2SiO_4$. This mineral constitutes the major proportion of the upper mantle. Olivine behavior, under pressure and temperature conditions relevant for the upper mantle, is complex, see *Karato and Wu* [1993] and *Hirth and Kohlstedt* [2003] for a review. We focus here on its behavior in the dislocation creep regime. Dynamic recrystallization affects both LPO development and grain size [*Zhang and Karato*, 1995; *Wenk and Tomé*, 1999; *Bresser et al.*, 2001]. Upwelling flow such as expected beneath mid-ocean ridges results in partial melting, which may reduce the viscosity and generate buoyancy forces [*Kohlstedt and Zimmerman*, 1996; *Braun et al.*, 2000; *Blackman and Kendall*, 1997]. Concerning dislocation creep, water fugacity has been shown to have a significant influence on the strength of the major slip

[1]Institution of Geophysics and Planetary Physics, Scripps Institution of Oceanography, University of California San Diego, La Jolla, California, USA.
[2]Laboratoire des Propriétés Mécaniques et Thermodynamiques des Matériaux, CNRS, Villetaneuse, France.
[3]Materials Science and Technology Division, Los Alamos National Laboratory, Los Alamos, New Mexico, USA.
[4]Department of Mechanical Engineering and Applied Mechanics, University of Pennsylvania, Philadelphia, Pennsylvania, USA.

0148-0227/08/2007JB005444$09.00

Table 1. List of Acronyms

LPO	Lattice Preferred Orientation
FFT	Fast Fourier Transform
SC	Self-Consistent Model
NPLCP	N-Phases Linear Comparison Polycrystal
TGT	Tangent Estimate
AFF	Affine Estimate
VAR	Variational Estimate
SO	Second-Order Estimate

systems. Slip along the [001] direction is enhanced with respect to slip along [100] by the addition of water, leading thus to different LPO development, and strain rate increases by a factor of 2∼6 [*Mackwell et al.*, 1985; *Karato et al.*, 1986; *Mei and Kohlstedt*, 2000; *Jung and Karato*, 2001]. Finally, recent experimental work at high pressure [*Couvy et al.*, 2004; *Raterron et al.*, 2007] together with atomistic simulations [*Durinck et al.*, 2005] indicate the dominant role of slip along [001] at pressures higher than ∼7 GPa. LPO produced by these deformation mechanisms may be consistent with seismological observations below 250 km depth [*Mainprice et al.*, 2005]. These processes could modify texture/rheologic effects due to dislocation controlled LPO, but a more quantitative understanding of the latter is an important framework to develop so that the scale of different factors can be reasonably compared in the future.

[4] Several polycrystal plasticity models have been applied to assess LPO development in olivine polycrystalline aggregates. The uniform stress model, used by *Chastel et al.* [1993] and *Dawson and Wenk* [2000], does the assumption that each grain of the polycrystal experiences uniform stress, so that grains poorly oriented for dislocation glide may not deform at all. This model provides a rather weak estimate for polycrystal behavior when the strength of all slip systems differ signficantly. It has been found in ice to underestimate significantly the overall anisotropy for pronounced LPO [*Castelnau et al.*, 1997]. The model of *Parks and Ahzi* [1990], and the kinematic model of *Ribe and Yu* [1991] which has been further extended by *Kaminski and Ribe* [2001], have been constructed especially to deal with polycrystals lacking five independent slip systems, such as olivine. The Kaminski-Ribe model has been employed in a number recent geophysical applications, since it can be fairly easily implemented in large-scale flow calculations, and its predictions for simple strain paths can reproduce key aspects of observed olivine behavior in laboratory experiments, with adjustment of one or two parameters. However, from a physical point of view, the most accurate micromechanical model to date for olivine aggregates [*Wenk et al.*, 1991; *Tommasi et al.*, 1999, 2000; *Blackman et al.*, 2002] was that based on the tangent extension of the Self-Consistent (SC) scheme proposed by *Molinari et al.* [1987], and generalized for anisotropic polycrystals by *Lebensohn and Tomé* [1993]. This is the so-called "VPSC model" in geophysical literature, here referred to as the tangent model (TGT), as explained below. This scheme has often been described as if the interaction between each grain and its surrounding could be approximated by the interaction between one ellipsoidal grain with the same lattice orientation as the original grain and a homogeneous equivalent medium whose behavior represents that of the polycrystal, taking thus advantage of the analytical solution of *Eshelby* [1957] for the inclusion/matrix interaction. This reasoning led to the conclusion that the TGT scheme implicitly considers uniform stress and strain rate inside grains.

[5] First, this interpretation of the TGT model turns out to be incorrect, since stress and strain rate heterogeneities within each crystal orientation (so-called "intraphase heterogeneity") do not vanish, see *Ponte Castañeda and Suquet* [1998] for a review. Next, an inconsistency in the TGT formulation, shown by *Masson et al.* [2000], explains why this approach tends to the uniform stress bound at large stress sensitivities, a limitation already pointed out by *Lebensohn and Tomé* [1993]. Following *Ponte Castañeda* [1996], *Masson et al.* [2000] further proposed an improved formulation (the "affine extension" of the SC scheme). In addition, two other major extensions of the SC scheme for polycrystals exhibiting nonlinear behavior have been proposed in recent years, namely the variational procedure (VAR) [*Ponte Castañeda*, 1991; *de Botton and Ponte Castañeda*, 1995] and the second order (SO) estimate [*Ponte Castañeda*, 2002a; *Liu and Ponte Castañeda*, 2004]. Both of them exhibit very interesting features, such as compliance with rigorous upper bounds for the effective potential, which are generally violated by other homogenization procedures [*Gilormini*, 1995]. This property ensures a more realistic averaging of the grain behavior during estimation of the polycrystal behavior. Applications of the VAR procedure to polycrystals with grains having cubic or hexagonal crystallographic structures can be found in [*Nebozhyn et al.*, 2001; *Liu et al.*, 2003a].

[6] In addition to these mean-field estimates, which are based on a statistical description of the microstructure, full-field approaches accounting for the exact polycrystal microstructure (if known) have been proposed to compute the fluctuation of the stress and strain rate inside grains, together with the overall polycrystal behavior. While such calculations are possible using the Finite Element Method [*Sarma and Dawson*, 1996; *Kanit et al.*, 2003], a numerically more efficient method based on Fast Fourier Transforms (FFT) has been proposed recently [*Moulinec and Suquet*, 1998], and applied to polycrystals [*Lebensohn*, 2001]. However, unlike mean-field approaches, the computation power required by these full-field approaches is far too large to imagine their coupling with a large-scale convection flow model for the upper mantle.

[7] There are two salient features in the aforementioned studies on olivine that are worth emphasizing. First, mean-field approaches have been applied to investigate the development of LPO, but the associated viscoplastic anisotropy of olivine aggregates has never been thoroughly studied, although this is certainly important for mantle convection where flow gradients are strong. Next, a challenging feature in olivine plasticity is the lack of five independent slip systems at the grain level, which, according to the von Mises criterion, are necessary to accommodate any arbitrary plastic deformation. According to [*Tommasi et al.*, 2000; *Wenk and Tomé*, 1999], the TGT model seems to work with only the main slip systems for olivine, providing thus only three independent systems, which is a puzzling result. It is however worth noting that

Table 2. Slip Plane (*hkl*) and Orientation of the Burgers Vector [*uvw*] Considered for Olivine Grains, Together With the Number of Equivalent Systems for Each Family (*k*) and the Reference Shear Stresses $\tau_{0(k)}$. The Last System of This Table is Added Only for the Sake of Having Five Independent Slip Systems at the Grains Scale

Slip System	Equiv.	$\tau_{0(k)}$
(010)[100]	1	τ_0
(001)[100]	1	τ_0
(010)[001]	1	$2\tau_0$
(100)[001]	1	$3\tau_0$
{011}[100]	2	$4\tau_0$
{031}[100]	2	$4\tau_0$
{110}[001]	2	$6\tau_0$
$\{111\}\langle 1\bar{1}0\rangle$	12[a]	$M\tau_0$

[a]Strictly speaking, these twelve systems are not equivalent owing to the orthorhombic structure of olivine crystals, but this distinction has not been considered here.

some polycrystals are able to deform with less than five independent systems. This is the case of hexagonal polycrystals with grains deforming by basal and prismatic slip only, i.e., with four independent systems [*Hutchinson*, 1977; *Nebozhyn et al.*, 2000]. However, this behavior is model-dependent [*Nebozhyn et al.*, 2001], its relevance for olivine needs to be investigated explicitly.

[8] The aim of this paper is to provide new insight into the rheological behavior of olivine polycrystals, based on micromechanical approaches. We focus on the effect of the lack of five independent slip system in terms of effective behavior at the polycrystal scale, but we also investigate the stress and strain rate distributions inside individual grains with different crystallographic orientations. We assess the relevance of several mean-field approaches for olivine, in view of the eventual desire to couple more accurate polycrystal deformation modeling with mantle convection calculations. It must be emphasized that, in the present work, LPO development at large strain is not investigated. We focus on the relation between the behavior of single grains and that of polycrystals. This work is therefore limited to the study of the *instantaneous* flow stress of polycrystals (i.e., corresponding to infinitesimal strain). For sake of simplicity, we also only consider isotropic polycrystals, i.e., exhibiting a random LPO. The development of LPO at large strain, and the subsequent evolving anisotropic behavior at the polycrystal scale will need to be tracked explicitly for a complete study, but this is left for future work. Furthermore, we will not perform here a detailed comparison to existing experimental data, which is another difficult task beyond the scope of this paper. Extensive experimental comparison at various pressure and temperature conditions will be investigated later. Therefore we will consider a simple but representative constitutive relation at the grain scale, presented in section 2. The full-field approach based on the FFT procedure will be presented and applied to obtain reference results on the behavior (section 3). In section 4, a description of the main features of several mean-field approaches based on the SC scheme will be given, for both linear and nonlinear viscoplastic polycrystals. The results of these SC estimates are compared to the reference FFT solutions (section 5) and discussed in terms of deformation characteristic of olivine polycrystals and compared to other known materials (section 6).

2. Grain Rheological Behavior

[9] At the grain (local) scale, we consider deformation that occurs only by dislocation creep on a given number of slip systems. The resolved shear stress $\tau_{(k)}$ acting on a slip system (*k*) is given by a projection of the local deviatoric stress tensor $\boldsymbol{\sigma}$

$$\tau_{(k)}(\mathbf{x}) = \boldsymbol{\mu}_{(k)}^{(r)} : \boldsymbol{\sigma}(\mathbf{x}) \tag{1}$$

with $\boldsymbol{\mu}_{(k)}^{(r)}$ the Schmid tensor expressing the orientation of the slip system with respect to a laboratory reference frame, (*r*) representing the crystal orientation at a given spatial position $\mathbf{x}$, and : denoting the product contracted on two indices. As for the constitutive relation at the slip system level, we use a classical power law for the slip-rate $\dot{\gamma}$ on system (*k*)

$$\dot{\gamma}_{(k)}(\mathbf{x}) = \dot{\gamma}_0 \left| \frac{\tau_{(k)}(\mathbf{x})}{\tau_{0(k)}} \right|^{n_{(k)}-1} \frac{\tau_{(k)}(\mathbf{x})}{\tau_{0(k)}} \tag{2}$$

with $\tau_{0(k)}$ a reference shear stress that expresses the "strength" of the system (*k*), $n_{(k)}$ the corresponding stress sensitivity, and $\dot{\gamma}_0$ a reference slip-rate. Combining all available slip systems, the local strain rate thus reads

$$\dot{\boldsymbol{\varepsilon}}(\mathbf{x}) = \sum_{k=1}^{K} \boldsymbol{\mu}_{(k)}^{(r)} \dot{\gamma}_{(k)}(\mathbf{x}) \tag{3}$$

with *K* the total number of slip systems.

[10] The dislocation slip systems considered here are those used by *Tommasi et al.* [2000] based on experimental results [*Durham et al.*, 1977; *Durham and Goetze*, 1977; *Bai et al.*, 1991; *Bai and Kohlstedt*, 1992]. They are listed in the first seven lines of Table 2, and illustrated in Figure 1. Subsets of the same systems were also used in different studies, e.g., [*Wenk and Tomé*, 1999; *Blackman et al.*, 2002; *Kaminski et al.*, 2004], with somewhat different $\tau_{0(k)}$. These

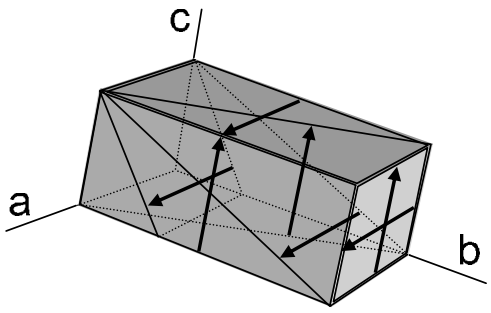

Figure 1. Schematic representation of slip systems in olivine single crystals.

slip systems represent material behavior sufficiently well that general conclusions can be drawn about grain-scale deformation and, thus, effective polycrystal response. Easy slip occurs in olivine along the [100] direction, whereas slip along the [001] direction is permitted, but with a higher resistance. These conditions are appropriate for "dry" crystals deformed at high temperature and low pressure. We have chosen the same stress sensitivity $n_{(k)} = n$ for all systems. This is a tendency that seems to come out of the experimental data, but note that this may not be a general behavior. The generally observed value, considered here, is $n = 3.5$. Such a value would indicate that creep is controlled by dislocation glide, with dislocation motion controlled by any of a number of numerous mechanisms [*Weertman*, 1975]. Typical values for τ_0 and $\dot{\gamma}_0$ for conditions prevailing in the upper mantle would be of the order of 1 MPa and 10^{-15} s^{-1}, respectively.

[11] Only three of these slip systems are independent. They allow shearing of the crystal lattice, but none of them allow axial deformation along the **a**, **b**, or **c** lattice directions. These systems thus cannot accommodate an arbitrary plastic deformation of olivine crystals, since five independent systems are required according to the von Mises criterion. Consequently, following the generally adopted procedure (see *Tommasi et al.* [2000] and *Wenk and Tomé* [1999], among others), we introduce an additional slip family $\{111\}\ \langle 1\bar{1}0\rangle$ for the sole purpose of having five independent systems at the crystal level. It should made be clear that this mode has not been observed in olivine, and its introduction in previous work was a purely numerical convenience. It is generally set stiff enough so that its influence on LPO development becomes negligible. In the following, we will however see that, using more sophisticated (and realistic) micromechanical models, as well as more subtle indicators for the mechanical state of the material, this artificial slip mode has a real influence on the behavior. In the present work, the desire of this implementation is to provide a rough representation of the accommodation processes in real olivine, such as grain boundary sliding or dislocation climb. The reference resolved shear stress for this system is given by the value of M (Table 2), denoted hereafter "anisotropy parameter", since M expresses part of the *local* viscoplastic anisotropy, i.e., at the grain scale. A high value of M corresponds to a large difference between normal and shear viscosity, and thus to a high anisotropy of grains. The limiting case of $M \to \infty$ is equivalent to removing this system, leaving the grain with infinite normal viscosities along the **a**, **b**, and **c** directions and an open yield surface. The reason for introducing this artificial slip family and not a more physically based accommodation mechanism is twofold. First, accommodation mechanisms in olivine are not well characterized experimentally. Diffusion processes, grain boundary sliding, and dislocation climb are however often evoked in the literature. Second, there are no micromechanical models available to date for polycrystal viscoplasticity accounting for more sophisticated deformation processes than regular dislocation glide on fixed lattice planes. Specific (and probably lengthy) developments are thus required in that field. The procedure followed here will however allow us to assess the relevance of different homogenization methods for olivine, and to shed light on the local mechanical state of polycrystal of olivine deforming in the dislocation creep regime.

3. Full-Field Computations

3.1. FFT-Based Formulation

[12] The FFT-based, full-field formulation for viscoplastic polycrystals, to be used as a reference solution for comparison with the results of statistical approaches, has been developed for periodic unit cells. It provides a solution of the governing equations (equilibrium and compatibility). It was originally developed as a fast algorithm to compute the elastic and elastoplastic effective and local responses of composites [*Moulinec and Suquet*, 1994, 1998; *Michel et al.*, 2000] and later generalized to deal with the viscoplastic deformation of polycrystals [*Lebensohn*, 2001].

[13] Briefly, the FFT-based formulation consists of finding a strain rate field associated with a kinematically admissible velocity field that minimizes the average local work-rate under the compatibility and equilibrium constraints. The method is based on the fact that the local mechanical response of a periodic heterogeneous medium can be calculated as a convolution integral between the Green function of a linear reference homogeneous medium and the actual heterogeneity field. Since such integrals reduce to a simple product in Fourier space, the Fast Fourier Transform algorithm can be used to transform the heterogeneity field into Fourier space and, in turn, get the mechanical fields by transforming that product back to real space. An iterative scheme must be implemented to obtain, upon convergence, a compatible strain rate field and a stress field in equilibrium, see [*Michel et al.*, 2000; *Lebensohn et al.*, 2004a] for details.

3.2. Microstructural Model

[14] In the full-field approach, the polycrystal microstructure has to be defined explicitly by specifying the arrangement and crystallographic orientations of the grains. Obviously, the reference solution provided by the FFT method corresponds to the considered microstructure. However, the microstructure of polycrystals is essentially *random* in nature (no correlation between the orientation of one particular grain, the orientation of the neighboor grains, the grain shape, ...). To capture this feature, the full-field method is used to perform a large number of computations on randomly generated microstructures, each single microstructure (denoted hereafter a "configuration") containing a reasonably small number of grains due to the obvious limitation associated with the size of computer memory. The desired results are obtained by taking an ensemble average over all configurations [*Kanit et al.*, 2003]. The more grains in each configuration and the more configurations considered, the more accurate the result is. To get a quantitative estimate of the significance of the results, the error associated with the ensemble average procedure is evaluated according to the method described by *Kanit et al.* [2003]. In all forthcoming figures, the obtained standard deviation of results is found to be always smaller than the size of the symbol used for the plots.

[15] The microstructures considered here are periodic three-dimensional unit-cells, randomly generated by Voronoi tessellation and containing 32 grains each. A typical micro-

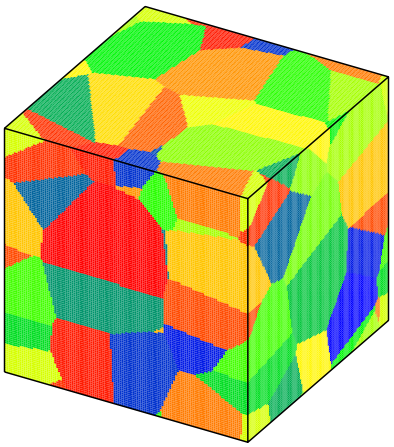

Figure 2. Typical periodic microstructure generated by Voronoi tesselation. It contains 32 grains, each having a different color that corresponds to its crystallographic orientation.

structure is illustrated in Figure 2. Ensemble average has been performed over $N = 50$ configurations. In order to make the comparison with mean-field approaches more accurate, the same crystallographic orientations for those 32 grains have been taken for all configurations. Grains orientations have been chosen in order to approach an isotropic behavior for the polycrystal; Euler angles have been selected in accordance with a quasi-random Sobol sequence [*Press et al.*, 1992], since the so-obtained orientation distribution has been found to exhibit a better isotropy than that given by the random orientation distribution generally used. For the FFT computations, a regular Fourier grid of $64 \times 64 \times 64$ points has been used to discretize the unit cell, leading to an average of 8192 Fourier points per grain.

3.3. Representative Results

[16] The computations of mechanical behavior were performed for uniaxial compression with an equivalent macroscopic strain rate $\dot{\bar{\varepsilon}}_{eq} = \dot{\gamma}_0$ where

$$\dot{\bar{\varepsilon}}_{eq} = \sqrt{2/3\dot{\bar{\varepsilon}} : \dot{\bar{\varepsilon}}} \tag{4}$$

and $\dot{\bar{\boldsymbol{\varepsilon}}}$ denotes the macroscopic strain rate tensor. In what follows, we calculated the mechanical behavior corresponding to a fixed configuration, with no evolution of the microstructure and/or the mechanical fields. Therefore only the instantaneous viscoplastic response of polycrystalline olivine will be investigated.

[17] Full-field approaches can be used advantageously to examine the distribution of the stress and strain rate within the microstructure. A 3-D overview of the distribution of the local equivalent strain rate $\dot{\varepsilon}_{eq}(\mathbf{x})$ is given in Figure 3 for anisotropy parameters $M = 10$ and $M = 100$, with

$$\dot{\varepsilon}_{eq}(\mathbf{x}) = \sqrt{2/3\dot{\varepsilon}(\mathbf{x}) : \dot{\varepsilon}(\mathbf{x})}. \tag{5}$$

[18] First, it can be seen that strong strain localization occurs. Strain is concentrated in bands located either within the grains or lying along grain boundaries, as observed experimentally in metallic aggregates [*Soppa et al.*, 2001]. The highest strain rates are found along grain boundaries. For $M = 10$, it is clear that some grains (the "soft" ones) exhibit higher average strain rate than others (the "hard" grains), but it is worth noting that all grains deform heterogeneously. For $M = 100$, the intragranular strain heterogeneity becomes very high and dominates over the intergranular heterogeneity. Values as high as $\dot{\varepsilon}_{eq}(\mathbf{x}) = 14\dot{\bar{\varepsilon}}_{eq}$ can be found locally. The average strain rate of each grain depends not only on its crystal orientation, but also depends strongly on the shape and orientation of its neighbors.

[19] To investigate these heterogeneities in more detail, the distribution of stress and strain rate are now considered. Figure 4 shows the probability density obtained for $\sigma_{eq}/\bar{\sigma}_{eq}$ and $\dot{\varepsilon}_{eq}/\dot{\bar{\varepsilon}}_{eq}$ in the softest of the 32 crystal orientations, with

$$\sigma_{eq}(\mathbf{x}) = \sqrt{3/2\sigma(\mathbf{x}) : \sigma(\mathbf{x})} \tag{6}$$

and similar definition for the macroscopic counterpart $\bar{\sigma}_{eq}$. Both stress and strain rate are very heterogeneously distributed, even for the relatively small local rheologic anisotropy $M = 10$. For $M = 100$, the width of the distribution is considerable. Some regions of grains do not deform at all ($\dot{\varepsilon}_{eq} \approx 0$) whereas other regions do deform up to $6 \sim 7$ times more rapidly than the macroscopic average. The local stress exhibits similar behavior, with sometimes very low (almost vanishing) values, and sometimes very

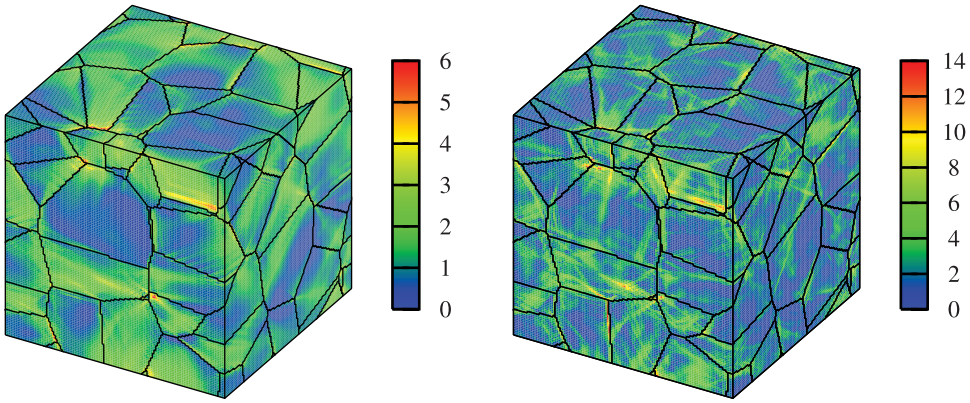

Figure 3. Spatial distribution of $\dot{\varepsilon}_{eq}/\dot{\bar{\varepsilon}}_{eq}$ calculated by the FFT method for (left) $M = 10$ and (right) $M = 100$, for the microstructure given in Figure 2. Solid lines indicate the grain boundaries (and cube edges). The direction of uniaxial tension is vertical. Note that scales are different on both figures.

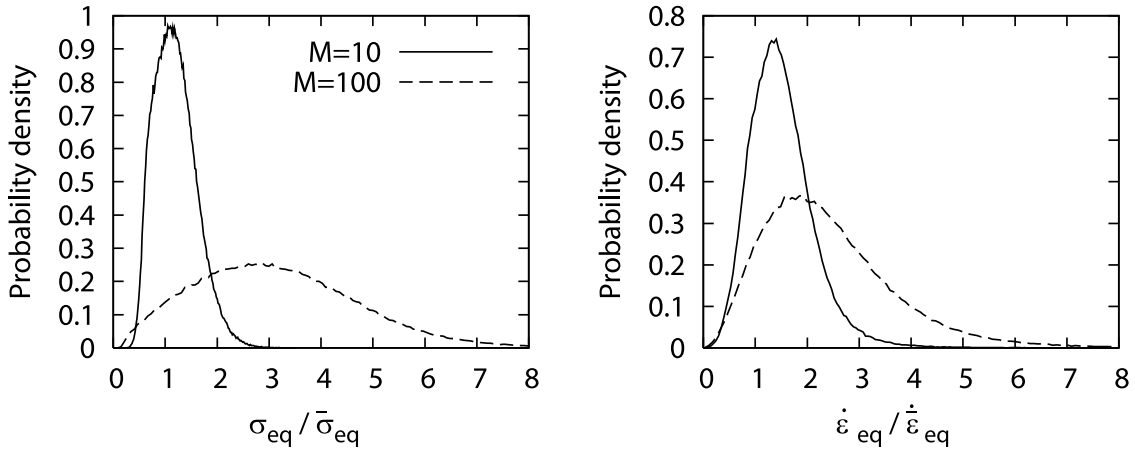

Figure 4. Distribution of normalized (left) equivalent stress and (right) equivalent strain rate, for $M = 10$ and $M = 100$, in a particular crystal orientation well oriented for slip along the easiest systems.

high values. Furthermore, the local quantities σ_{eq} and $\dot{\varepsilon}_{eq}$ are on average significantly larger than their macroscopic counterpart, $\bar{\sigma}_{eq}$ and $\bar{\dot{\varepsilon}}_{eq}$. For $M = 100$, the average of σ_{eq} is about $3 \times \bar{\sigma}_{eq}$; even in this crystal orientation favorable for deformation, the equivalent stress within grains can be much larger than the macroscopic value. This illustrates the fact that individual grains are subjected to stress regimes significantly different from the uniaxial compression prescribed macroscopically. Similar behavior has also been observed for the other crystal orientations, not reported here for sake of brevity.

[20] Figure 5 shows the distributions of the resolved shear stress τ and shear-rate $\dot{\gamma}$ on the easiest slip system of the same crystal orientation. Again, the large width of the distributions, increasing with M, is noticeable. In fact, τ and $\dot{\gamma}$ distributions are not independent, they are linked by the local constitutive relation (2). A remarkable result, which is due to the nonlinearity of the behavior, is that these distributions do not exhibit the same shape. This is particularly evident for $M = 100$, where the unimodal distribution of $\dot{\gamma}$ is associated with a bimodal distribution of τ. Moreover, from purely geometrical considerations, according to the orientation of the slip system with respect to the applied deformation rate, it is expected that the system glides with τ and $\dot{\gamma}$ both positive. Clearly, this is not the case at high anisotropy parameter. This system, which is among the softest in the whole polycrystal, slips frequently in a direction opposite to the one expected intuitively. This highlights the very strong influence of neighbor grains on the local stress and strain conditions.

[21] Similar conclusions can be drawn for "hard glide" conditions, i.e., when the crystal orientation is such that a given slip plane is normal to the applied macroscopic compressive stress, leading thus to vanishing *average* shear stress and shear-rate. In that case, it can be shown that the *local* shear stress on that system is generally significant, leading to *local* shear-rates $\dot{\gamma}$ up to $5 \times \dot{\gamma}_0$ for $M = 100$ [see also *Castelnau et al.*, 2006]. In other words, local grain interactions allow even unfavorably oriented slip systems to become susceptible to significant local activation.

4. Mean-Field Estimates

[22] Unlike full-field approaches, mean-field methods are based on a statistical description of the microstructure of the polycrystalline aggregate. The microstructure is described

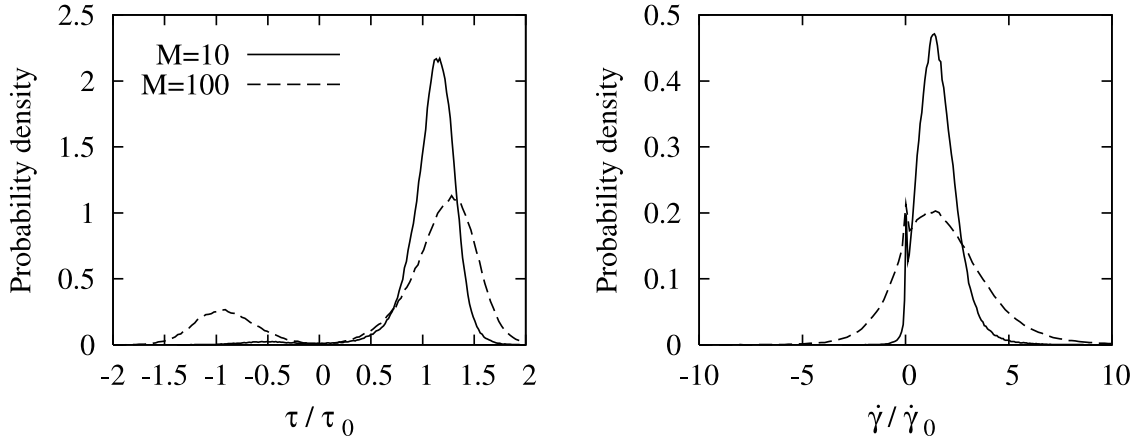

Figure 5. Distribution of normalized resolved (left) shear stress and (right) shear-rate, for $M = 10$ and $M = 100$, on the easy slip system (010)[100] of the same (soft) crystal orientation as in Figure 4.

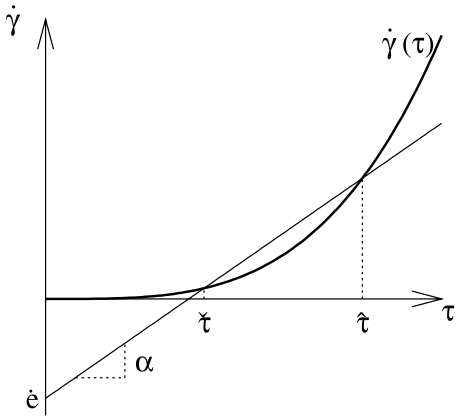

Figure 6. Schematic representation of the linearization (12).

by several *n*-points correlation functions, so that the exact position and shape of one grain with respect to its neighbors is not known. However, all grains exhibiting the same crystallographic orientation are treated as a single "mechanical phase", also called "crystal orientation" hereafter. Such a phase thus regroups many (in fact an infinite number of) grains of similar orientation, but with different shape and surroundings. This procedure would correspond to ensemble averaging over a sufficiently large number of FFT configurations.

[23] Owing to the random character of the microstructure in polycrystals with all grains playing geometrically similar roles, the Self-Consistent (SC) scheme [*Hershey*, 1954; *Kröner*, 1958, 1978; *Willis*, 1981] is especially well suited for these materials. The SC scheme was originally developed for materials exhibiting *linear* behavior. The basic method to deal with *nonlinear* behavior such as viscoplasticity is to define an "N-Phase Linear Comparison Polycrystal" (NPLCP) having the same microstructure as the real nonlinear polycrystal, and to which the SC scheme can be applied in order to get the behavior of the real polycrystal. Of course, the so-estimated effective behavior remains nonlinear since the definition of the NPLCP depends on the applied macroscopic strain rate. The difficult part of the problem consists of finding the "right" linearization procedure leading to the optimal selection of the NPLCP. In the following, after briefly reviewing the main features of the (linear) SC scheme, several *extensions* of the SC scheme for viscoplasticity are briefly described.

4.1. Exact Solution for Linear Viscosity

[24] For reasons that will become evident in the sequel, we deal here with materials exhibiting the following linear behavior at the local scale

$$\dot{\boldsymbol{\varepsilon}}(\mathbf{x}) = \mathbf{M}^{(r)} : \boldsymbol{\sigma}(\mathbf{x}) + \dot{\boldsymbol{\varepsilon}}_0^{(r)} \tag{7}$$

with $\mathbf{M}^{(r)}$ a viscous compliance and $\dot{\boldsymbol{\varepsilon}}_0^{(r)}$ a stress-free strain rate, which are both *homogeneous in crystal orientation* (*r*). It is known [e.g., *Ponte Castañeda and Suquet*, 1998] that the effective behavior exhibits the same form

$$\dot{\bar{\boldsymbol{\varepsilon}}} = \tilde{\mathbf{M}} : \bar{\boldsymbol{\sigma}} + \dot{\bar{\boldsymbol{\varepsilon}}}_0 \tag{8}$$

where the macroscopic stress $\bar{\boldsymbol{\sigma}}$ and macroscopic strain rate $\dot{\bar{\boldsymbol{\varepsilon}}}$ are defined by the average over the whole polycrystal volume (denoted $\langle . \rangle$) of the corresponding local quantities

$$\bar{\boldsymbol{\sigma}} = \langle \boldsymbol{\sigma}(\mathbf{x}) \rangle, \quad \dot{\bar{\boldsymbol{\varepsilon}}} = \langle \dot{\boldsymbol{\varepsilon}}(\mathbf{x}) \rangle. \tag{9}$$

The effective compliance $\tilde{\mathbf{M}}$ and the effective stress-free strain rate $\dot{\bar{\boldsymbol{\varepsilon}}}_0$ are given by the following exact relations

$$\tilde{\mathbf{M}} = \langle \mathbf{M}(\mathbf{x}) : \mathbf{B}(\mathbf{x}) \rangle, \quad \dot{\bar{\boldsymbol{\varepsilon}}}_0 = \langle \dot{\boldsymbol{\varepsilon}}_0(\mathbf{x}) : \mathbf{B}(\mathbf{x}) \rangle \tag{10}$$

where $\mathbf{B}$ is the stress localization tensor. Since $\mathbf{M}$ and $\dot{\boldsymbol{\varepsilon}}_0$ are both uniform per phase, the knowledge of the phase averages of $\mathbf{B}$, denoted $\mathbf{B}^{(r)}$, are sufficient to solve the equation (10). For the SC scheme, which provides the exact solution for some specific random microstructures, expressions for $\mathbf{B}^{(r)}$ in a general context of anisotropy can be found, e.g., by *Brenner et al.* [2004].

[25] With this in hand, statistical averages over the crystal orientations can be estimated. Basically, two quantities can be obtained. The phase average stress (or first moment) $\boldsymbol{\sigma}^{(r)}$, defined as $\boldsymbol{\sigma}^{(r)} = \langle \boldsymbol{\sigma} \rangle^{(r)}$ with $\langle . \rangle^{(r)}$ the average over the volume of crystal orientation (*r*), is directly related to the stress concentration tensor

$$\boldsymbol{\sigma}^{(r)} = \mathbf{B}^{(r)} : \bar{\boldsymbol{\sigma}} + \boldsymbol{\sigma}_{\text{res}}^{(r)}, \tag{11}$$

with $\boldsymbol{\sigma}_{\text{res}}^{(r)}$ the residual stress. The knowledge of $\boldsymbol{\sigma}^{(r)}$ for all crystal orientations (*r*) allows investigation of the so-called "interphase" heterogeneities, i.e., the variation of the phase average stress with respect to the crystal orientation. Deeper insight into the stress distribution can be obtained from the second moment $\langle \boldsymbol{\sigma} \otimes \boldsymbol{\sigma} \rangle^{(r)}$ ($\otimes$ denotes the dyadic product), which is simply the tensorial expression for the mean of the square of the stress. It can be obtained by the method presented by *Bobeth and Diener* [1987] and *Kreher* [1990]. Note that the variance of the stress within a given crystal orientation can be estimated from these two quantities as $\langle \boldsymbol{\sigma} \otimes \boldsymbol{\sigma} \rangle^{(r)} - \langle \boldsymbol{\sigma} \rangle^{(r)} \otimes \langle \boldsymbol{\sigma} \rangle^{(r)}$, which is related to the width of the stress distribution in crystal orientation (*r*). Similar relations can be derived for the strain rate statistics.

4.2. Approximate Solutions for Nonlinear Viscoplasticity

[26] To *generalize* the SC scheme for viscoplasticity, the local constitutive relation given by equations (1–3) has to be linearized in a suitable way to obtain a form similar to (7), with $\mathbf{M}^{(r)}$ and $\dot{\boldsymbol{\varepsilon}}_0^{(r)}$ uniform per phase. Generally speaking, the linearization of (2) can be expressed in the form depicted in Figure 6 [*Liu and Ponte Castañeda*, 2004]

$$\dot{\gamma}_{(k)}(\mathbf{x}) = \alpha_{(k)}^{(r)} \tau_{(k)}(\mathbf{x}) + \dot{e}_{(k)}^{(r)}, \tag{12}$$

thus leading to the following expressions for $\mathbf{M}^{(r)}$ and $\dot{\boldsymbol{\varepsilon}}_0^{(r)}$

$$\begin{aligned} \mathbf{M}^{(r)} &= \textstyle\sum_k \alpha_{(k)}^{(r)} \boldsymbol{\mu}_{(k)}^{(r)} \otimes \boldsymbol{\mu}_{(k)}^{(r)} \\ \dot{\boldsymbol{\varepsilon}}_0^{(r)} &= \textstyle\sum_k \dot{e}_{(k)}^{(r)} \boldsymbol{\mu}_{(k)}^{(r)} \end{aligned} \tag{13}$$

Without loss of generality, the shear compliance $\alpha_{(k)}^{(r)}$ and stress-free shear-rate $\dot{e}_{(k)}^{(r)}$ can be expressed with respect to two reference shear stresses, $\check{\tau}_{(k)}^{(r)}$ and $\hat{\tau}_{(k)}^{(r)}$, as

$$\alpha = \frac{\dot{\gamma}(\hat{\tau}) - \dot{\gamma}(\check{\tau})}{\hat{\tau} - \check{\tau}} \qquad \dot{e} = \dot{\gamma}(\check{\tau}) - \alpha\check{\tau} \tag{14}$$

where subscripts (k) and (r) have been omitted for clarity, and $\dot{\gamma}(\tau)$ denoting the shear-rate given by the nonlinear relation (2) for the shear stress τ. The optimal choice (from the point of view of the variational mechanical problem) of the reference stresses $\check{\tau}_{(k)}^{(r)}$ and $\hat{\tau}_{(k)}^{(r)}$ is not straightforward, and this is mainly the reason why several extensions of the SC scheme for viscoplasticity have been proposed in the literature. Basically, these different approaches can be distinguished by the corresponding choice of $\check{\tau}_{(k)}^{(r)}$ and $\hat{\tau}_{(k)}^{(r)}$. Obviously, all of them reduce to the same SC model in the linear case $n = 1$.

[27] Following *Ponte Castañeda* [1996], *Masson et al.* [2000] proposed the so-called "affine" (AFF) linearization scheme which is based on the simple and intuitive idea of a linear behavior (12) tangent to the nonlinear one (2) at the mean shear stress, leading to

$$\check{\tau}_{(k)}^{(r)} = \hat{\tau}_{(k)}^{(r)} = \langle \tau_{(k)} \rangle^{(r)}, \quad \alpha_{(k)}^{(r)} = \left. \frac{\partial \dot{\gamma}}{\partial \tau} \right|_{\tau = \check{\tau}_{(k)}^{(r)}}. \tag{15}$$

The main limitations of this procedure are discussed in detail by *Bornert and Ponte Castañeda* [1998] and *Masson et al.* [2000]. One of them is the violation of rigourous upper bounds for the effective behavior. More generally, the affine extension is known to overestimate the overall viscosity, i.e., to predict effective behavior that is too stiff. This negative feature can be alleviated by means of the energy formulation originally proposed by *Ponte Castañeda* [1996] [see *Bornert et al.*, 2001].

[28] Alternative, more sophisticated ways to generalize the SC scheme have been proposed by Ponte Castañeda and coworkers during the last decade. The basic idea of these methods is to guide the choice of the properties of the NPLCP by a suitably designed variational principle. More precisely, the trial fields in these variational principles are the shear compliances $\alpha_{(k)}^{(r)}$, while the constraints of stress equilibrium and strain compatibility are enforced through the NPLCP.

[29] For specific classes of NPLCP, an "optimal" solution has been obtained in the context of the so-called "variational" procedure (VAR) of *Ponte Castañeda* [1991], which was extended to polycrystals by *de Botton and Ponte Castañeda* [1995], leading to the choices

$$\check{\tau}_{(k)}^{(r)} = 0, \quad \hat{\tau}_{(k)}^{(r)} = \left[\langle \tau_{(k)}^2 \rangle^{(r)} \right]^{1/2} \tag{16}$$

and thus

$$\dot{e}_{(k)}^{(r)} = 0, \quad \alpha_{(k)}^{(r)} = \frac{\dot{\gamma}_0}{\tau_{0(k)}} \left| \frac{\check{\tau}_{(k)}^{(r)}}{\tau_{0(k)}} \right|^{n-1}. \tag{17}$$

Since $\dot{e}_{(k)}^{(r)} = 0$, this procedure can be interpreted as "generalized secant" linearization [*Suquet*, 1995]. In addition, it has been shown to provide a rigourous bound for the effective potential.

[30] More recently, the "second-order" (SO) method of *Ponte Castañeda* [2002a], extended to polycrystals by *Liu and Ponte Castañeda* [2004], has been proposed. It is based on the same variational procedure as VAR, except that the chosen NPLCP is not of the generalized secant type, but of a generalized affine type, not requiring the $\dot{e}_{(k)}^{(r)}$ to vanish. The original procedure consists of estimating the effective stress potential $\tilde{U}$ from which the effective strain rate can be derived, $\dot{\bar{\boldsymbol{\varepsilon}}} = \partial \tilde{U} / \partial \bar{\sigma}$. The application of this method to anisotropic polycrystals, for which the form of $\tilde{U}$ is not known in advance, would thus require a numerical differentiation of $\tilde{U}$ which may be rather laborious. Therefore use is made here of an approximation of the original SO formulation which aims at evaluating the effective behavior directly without having to know the effective potential. This provides slightly less accurate results than the original formulation [*Liu and Ponte Castañeda*, 2004], but is much more efficient from the computational point of view. The reference shear stresses now read

$$\check{\tau}_{(k)}^{(r)} = \langle \tau_{(k)} \rangle^{(r)}, \quad \hat{\tau}_{(k)}^{(r)} = \check{\tau}_{(k)}^{(r)} \pm \left[\langle \left(\tau_{(k)} - \check{\tau}_{(k)}^{(r)} \right)^2 \rangle^{(r)} \right]^{0.5} \tag{18}$$

where the + sign in the second equation has to be taken when $\check{\tau}_{(k)}^{(r)} > 0$, and the - when $\check{\tau}_{(k)}^{(r)} < 0$.

[31] For practical purposes, the main differences between AFF, VAR, and SO models may be summarized as follows. The AFF estimate can be regarded as a relatively simple model, allowing rapid computations which can even be rather accurate for polycrystals with weak grain anisotropy and small stress sensitivity. However, its predictions can become unrealistic (e.g., bound violation) at strong anisotropy or nonlinearity. The VAR and SO procedures clearly need more numerical effort, since they both require the computation of the second moments $\langle \boldsymbol{\sigma} \otimes \boldsymbol{\sigma} \rangle^{(r)}$. The VAR method provides a rigourous bound for the effective behavior, and can therefore improve on the AFF estimate at high anisotropy and nonlinearity. On the other hand, the SO procedure has been constructed to provide the best estimate of the effective behavior. In particular, by construction, it always complies with the VAR bound. It is therefore physically a more satisfying formulation.

[32] Finally, the "tangent" (TGT) extension of the SC scheme [*Molinari et al.*, 1987; *Lebensohn and Tomé*, 1993] is based on the same tangent linearization (15) as the AFF method. However, unlike the AFF extension, this procedure takes advantage of the fact that, for power law polycrystals with a single stress exponent n, the tangent behavior (12) can be replaced by a secant-like relation, with $\dot{e}_{(k)}^{(r)} = 0$ and $\alpha_{(k)}^{(r)}$ replaced by $n\alpha_{(k)}^{(r)}$. The same procedure is further applied at the macroscopic level, leading to an inconsistent definition for the stress localization tensor $\mathbf{B}^{(r)}$ that combines a secant description for the local and global behaviors but a tangent analysis for the inclusion/matrix interaction. When expressed in the form of tangent expressions, it can be shown that $\dot{\bar{\boldsymbol{\varepsilon}}}_0$ differs from the exact relation given in (10) [*Masson et al.*, 2000]. It is recalled that this TGT extension

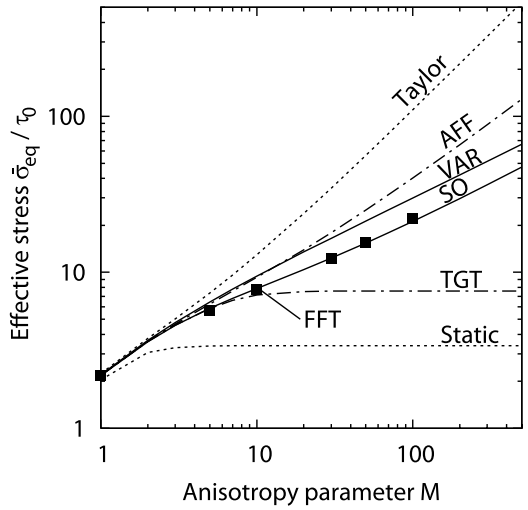

Figure 7. Effect of the anisotropy parameter M on the effective stress for several extensions of the SC scheme and compared to the reference solutions provided by the FFT full-field modeling. Static and Taylor bounds are also indicated.

was the most advanced micromechanical model applied to olivine to date.

5. Results

[33] The various extensions of the SC scheme were applied to a polycrystal made of the same 32 crystal orientations (or mechanical phases) as used for the full-field computations, and exhibiting the same (spherical) average grain shape. Recall that computations have been performed for a given effective strain rate $\bar{\dot{\varepsilon}}_{eq} = \dot{\gamma}_0$ under uniaxial compression. In addition to the SC schemes, results will be also given for the uniform stress (Static) and the uniform strain rate (Taylor) bounds. These latter two models are obtained by prescribing $\boldsymbol{\sigma}(\mathbf{x}) = \bar{\boldsymbol{\sigma}}$ and $\dot{\boldsymbol{\varepsilon}}(\mathbf{x}) = \bar{\dot{\boldsymbol{\varepsilon}}}$, respectively. They both predict homogeneous intraphase stress and strain rate. Our strategy is to present results concerning not only the effective behavior, but also the partitioning of stress and strain rate in the different crystal orientations, in order to show the levels of accuracy of the different mean-field approaches, and to better understand the rheological behavior of olivine.

[34] Figure 7 shows the equivalent effective stress $\bar{\sigma}_{eq}/\tau_0$ predicted by the TGT, AFF, VAR, and SO extensions of the SC scheme, as a function of the anisotropy parameter M. Results are compared to the reference solution provided by the FFT full-field approach. First of all, it is observed that the FFT approach indicates an effective stress increasing continuously with M. At sufficiently large local anisotropy, say $M > 10$, a rather simple scaling law is observed, with $\bar{\sigma}_{eq}/\tau_0$ being proportional to M^k, with $k \simeq 0.5$. The TGT extension of the SC scheme, on the other hand, shows a saturation of $\bar{\sigma}_{eq}/\tau_0$ still at moderate values of M ($\simeq$20) which clearly departs from the reference FFT results. Since $\bar{\sigma}_{eq}/\tau_0$ remains finite when $M \to \infty$, the TGT model allows the polycrystal to deform with only three independent slip systems. It thus behaves qualitatively like the Static bound, but with a higher flow stress. As expected, the Taylor bound significantly overestimates the effective stress which simply tends to be proportional to $M(k \simeq 1)$. The AFF formulation provides significantly better match to the full-field solution compared to the TGT model, at no additional numerical cost. However, the AFF flow stress increases too rapidly with M ($k \simeq 0.7$), and therefore the predictions become too stiff at large M. On the other hand, the predictions of the SO reproduce the FFT reference results almost perfectly. The VAR estimate is not as good a match to the full-field results as the SO prediction, being overly stiff. However, unlike all other models, both SO and VAR extensions predict the correct scaling with $k \simeq 0.5$.

[35] Figure 8 shows the evolution with M of the overall (normalized) stress and strain rate heterogeneities $\Sigma(\sigma_{eq})/\bar{\sigma}_{eq}$ and $\Sigma(\dot{\varepsilon}_{eq})/\bar{\dot{\varepsilon}}_{eq}$, which are defined as

$$\begin{aligned} \Sigma(\sigma_{eq}) &= \sqrt{\langle \sigma_{eq}^2 \rangle - \bar{\sigma}_{eq}^2} \\ \Sigma(\dot{\varepsilon}_{eq}) &= \sqrt{\langle \dot{\varepsilon}_{eq}^2 \rangle - \bar{\dot{\varepsilon}}_{eq}^2} \end{aligned} . \tag{19}$$

These quantities are related to the standard deviation of stress and strain rate in the whole polycrystal. They illustrate the *overall* heterogeneities in the polycrystal, combining the field fluctuations inside the grains together with the fluctuations between different grains. Note that only normalized results are presented in Figure 8 (and also in the forthcoming figures), with a normalization factor depending on the considered model. For example, $\Sigma(\sigma_{eq})/\bar{\sigma}_{eq}$ for the AFF model has been calculated using the AFF estimate for $\bar{\sigma}_{eq}$. The discrepancies concerning the effective flow stress, already discussed above (Figure 7), have thus to be taken into account to compare nonnormalized values (i.e., $\Sigma(\sigma_{eq})$). However, as for $\Sigma(\dot{\varepsilon}_{eq})/\bar{\dot{\varepsilon}}_{eq}$, since the same $\bar{\dot{\varepsilon}}_{eq}$ has been prescribed for all models, curves showing $\Sigma(\dot{\varepsilon}_{eq})/\bar{\dot{\varepsilon}}_{eq}$ and $\Sigma(\dot{\varepsilon}_{eq})$ exhibit similar shapes. It can be seen in Figure 8 that, similar to the effective behavior, the full-field solution predicts that stress and strain rate heterogeneities increase with the anisotropy parameter M. Again, the TGT approach exhibits a very different response, with a saturation at M values as small as $\sim$5–10. At large M, this approach predicts values of heterogeneities Σ that are very similar to the Taylor and Static bounds for the stress and the strain rate, respectively. (Note in passing that Static and Taylor bounds lead to $\Sigma(\sigma_{eq}) = 0$ and $\Sigma(\dot{\varepsilon}_{eq}) = 0$, respectively, by construction.) Moreover, the TGT model significantly overestimates $\Sigma(\dot{\varepsilon}_{eq})/\bar{\dot{\varepsilon}}_{eq}$ for M smaller than $\sim$10. On the other hand, the AFF, VAR, and SO estimates provides similar trends, in good agreement with full-field results (again, recall that we are dealing with normalized quantities). For $\Sigma(\sigma_{eq})/\bar{\sigma}_{eq}$, results are also very good quantitatively. As for $\Sigma(\dot{\varepsilon}_{eq})/\bar{\dot{\varepsilon}}_{eq}$, the prediction is slightly too large compared to full-field results. The best agreement is obtained here for the VAR model.

[36] We now investigate the distribution of stress and strain rate in the different crystal orientations. Figure 9 illustrates how the (normalized) average equivalent stress $\sigma_{eq}^{(r)}/\bar{\sigma}_{eq}$ and strain rate $\dot{\varepsilon}_{eq}^{(r)}/\bar{\dot{\varepsilon}}_{eq}$ are distributed in the different crystal orientations, for $M = 100$. The quantities $\sigma_{eq}^{(r)}$ and $\dot{\varepsilon}_{eq}^{(r)}$ are the von Mises equivalent stress and strain rate, e.g.

$$\sigma_{eq}^{(r)} = \sqrt{3/2 \langle \boldsymbol{\sigma} \rangle^{(r)} : \langle \boldsymbol{\sigma} \rangle^{(r)}}, \tag{20}$$

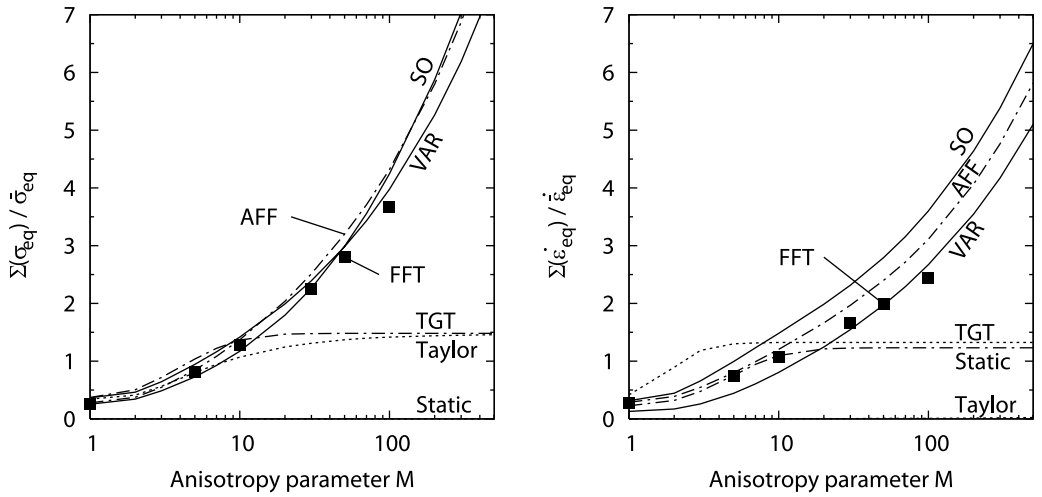

Figure 8. Normalized heterogeneities of (left) equivalent stress and (right) equivalent strain rate as a function of the anisotropy parameter M for several extensions of the SC scheme and compared to the reference solutions provided by the FFT full-field modeling. Static and Taylor bounds are also indicated.

i.e., they express the average stress and strain rate in the considered crystal orientation (r). Since the distributions of $\sigma_{eq}^{(r)}$ and $\dot{\varepsilon}_{eq}^{(r)}$ exhibit transverse isotropy with respect to the macroscopic compression axis, they can be fully represented in a single inverse pole figure of the compression axis. The lower left corner of these figures indicates values of $\sigma_{eq}^{(r)}/\bar{\sigma}_{eq}$ and $\dot{\varepsilon}_{eq}^{(r)}/\dot{\bar{\varepsilon}}_{eq}$ for crystal orientations exhibiting a [001] lattice direction aligned with the macroscopic compression axis. Similarly, the lower right corner indicates the values in those crystals having a [100] direction aligned with the compression axis, and so on. The reference full-field results indicate that hard grains are those for which one of the $\langle 001 \rangle$ crystal axis is aligned with the macroscopic compression axis. These grains experience a large average equivalent stress, up to 2.6 times larger than the macroscopic average $\bar{\sigma}_{eq}$, and a small equivalent strain rate which can be less than $0.4 \times \dot{\bar{\varepsilon}}_{eq}$. Soft orientations correspond to grains for which the macroscopic compression axis lies close to the $\langle 111 \rangle$ crystallographic direction. The corresponding grains experience small equivalent stress, which can be as small as $0.3 \times \bar{\sigma}_{eq}$, together with a high equivalent strain rate, up to $1.4 \times \dot{\bar{\varepsilon}}_{eq}$. The predictions of the TGT extension only roughly matches the reference full-field results. Particularly, the amplitudes of fluctuations are not correct, being overly small (large) for the stress (strain rate). Also, $\dot{\varepsilon}_{eq}^{(r)}$ displays excessive values for crystals with [110] or [101] lattice direction aligned with the macroscopic compressive axis. On the other hand, the AFF, VAR, and SO estimates all provide excellent results, virtually indistinguishable from the full-field predictions, except maybe for a slight underestimation of $\dot{\varepsilon}_{eq}^{(r)}$ for grains in the [100] direction. Both the shape of the distribution and the range of fluctuation are very well captured by these three approaches.

[37] Figure 10 shows the distribution of the normalized *intra*phase heterogeneities of stress $\Sigma^{(r)}(\sigma_{eq})/\bar{\sigma}_{eq}$ and strain rate $\Sigma^{(r)}(\dot{\varepsilon}_{eq})/\dot{\bar{\varepsilon}}_{eq}$, with

$$\Sigma^{(r)}(\sigma_{eq}) = \sqrt{\langle \sigma_{eq}^2 \rangle^{(r)} - \left(\sigma_{eq}^{(r)}\right)^2} \tag{21}$$

(and similarly for $\Sigma^{(r)}(\dot{\varepsilon}_{eq})$). These quantities reflect the width of the stress and strain rate distribution inside a given crystal orientation (r). Note that they vanish for both Static and Taylor bounds since stress and strain are assumed uniform inside grains in these models. The full-field results indicate that both $\Sigma^{(r)}(\sigma_{eq})/\bar{\sigma}_{eq}$ and $\Sigma^{(r)}(\dot{\varepsilon}_{eq})/\dot{\bar{\varepsilon}}_{eq}$ exhibit a rather poor dependence on the crystal orientations, with predicted values being almost constant and equal to about 3.4 and 2.3, respectively. The TGT approach displays a good qualitative match to the distribution of $\Sigma^{(r)}(\sigma_{eq})/\bar{\sigma}_{eq}$, also with almost constant values, but the strain rate intraphase heteogeneity $\Sigma^{(r)}(\dot{\varepsilon}_{eq})/\dot{\bar{\varepsilon}}_{eq}$ exhibits much greater fluctuations than the full-field prediction. In addition, this approach significantly underestimates both heterogeneities, the predicted values being only half those of the full-field solution. Since $\bar{\sigma}_{eq}$ is rather small for the TGT model (Figure 7), the nonnormalized value $\Sigma^{(r)}(\sigma_{eq})$ is as low as 6 times less than the FFT-based prediction. The AFF estimate predicts globally the correct level for $\Sigma^{(r)}(\sigma_{eq})/\bar{\sigma}_{eq}$ and $\Sigma^{(r)}(\dot{\varepsilon}_{eq})/\dot{\bar{\varepsilon}}_{eq}$, but the dependence on the crystal orientation is much larger than is obtained for the full-field method. Again, the best qualitative and quantitative agreement is obtained for the VAR and SO estimates. The obtained values of $\Sigma^{(r)}(\sigma_{eq})/\bar{\sigma}_{eq}$ and $\Sigma^{(r)}(\dot{\varepsilon}_{eq})/\dot{\bar{\varepsilon}}_{eq}$ do not depend on the crystal orientation, as anticipated. The predicted levels are also in good agreement with the full-field solution. The VAR procedure produces results in perfect agreement, and the SO extension slightly overestimates the intraphase strain rate heterogeneity. Note however that the VAR procedure overestimates the *nonnormalized* stress fluctuation $\Sigma^{(r)}(\sigma_{eq})$.

6. Discussion

[38] In this section, we analyze the results of the previous section with the objective of drawing some conclusions on the relevance of mean-field approaches for micromechanical modeling of olivine, the deformation mechanisms in olivine, and the subsequent coupling of the micromechanical model with a large-scale convection model for the upper mantle.

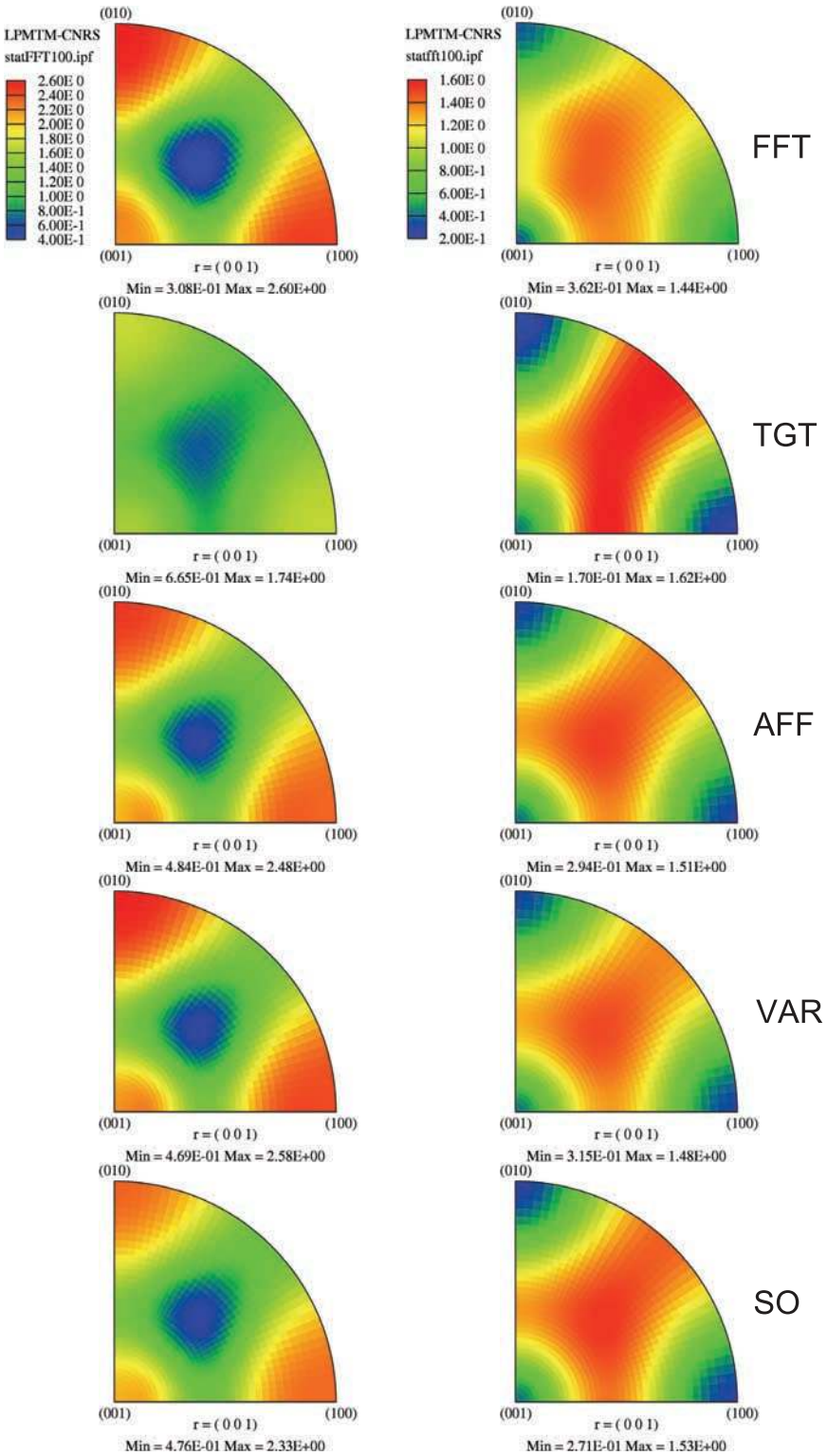

Figure 9. Inverse pole figures of the uniaxial compression axis showing the distribution of the normalized average equivalent (left) stress $\sigma_{eq}^{(r)}/\bar{\sigma}_{eq}$ and (right) strain rate $\dot{\varepsilon}_{eq}^{(r)}/\bar{\dot{\varepsilon}}_{eq}$ in crystal axes, for the FFT, TGT, AFF, VAR, and SO estimates, and $M = 100$. Color codes used for both quantities are shown on top of the figure.

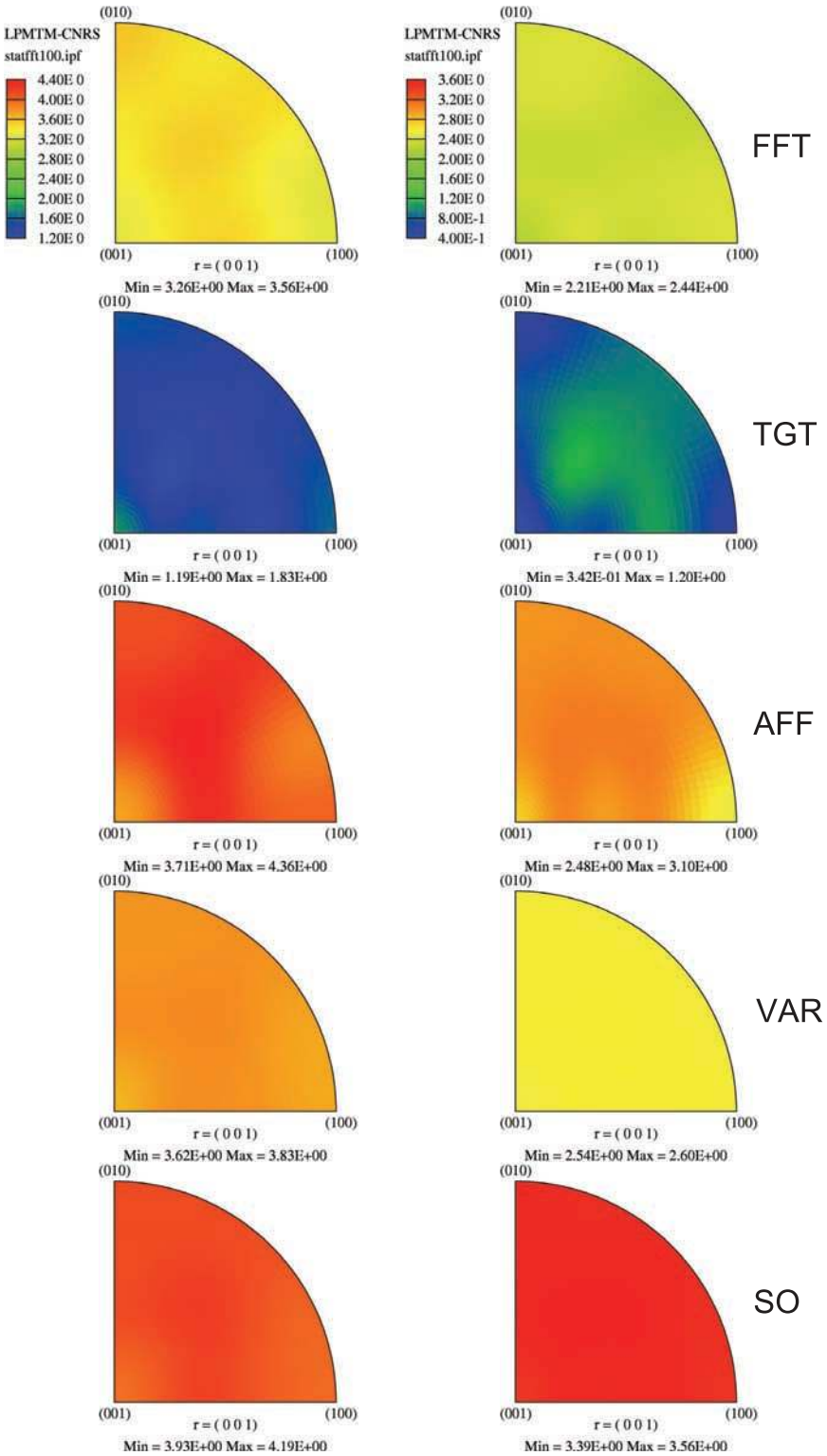

Figure 10. Inverse pole figures of the uniaxial compression axis showing the distribution of the *intra*phase heterogeneity of (left) stress $\Sigma^{(r)}(\sigma_{eq})/\bar{\sigma}_{eq}$ and (right) strain rate $\Sigma^{(r)}(\dot{\varepsilon}_{eq})/\bar{\dot{\varepsilon}}_{eq}$ in crystal axes, for the FFT, TGT, AFF, VAR, and SO estimates, and $M = 100$. Color codes used for both quantities are shown on top of the figure.

6.1. Relevance of the Mean-Field Approaches

[39] When comparing the predictions of nonlinear extensions of the SC scheme to reference results obtained by the full-field FFT approach, there are two major sources of discrepancy [*Rekik et al.*, 2006]. The first source concerns the effect of the linearization procedure. The second is associated with the microstructures of the considered polycrystals. To a lesser extent, part of the discrepancy might be also related to the unavoidable inaccuracies of the full-field solutions at large M, due to the finite size of the FFT grid, but this last source is believed to remain minimal here, except maybe for the case of the strain rate fluctuations for high values of M, in which slight inaccuracy of reference solutions could be expected [*Lebensohn et al.*, 2004b].

[40] The full-field simulations provides a solution for a randomly generated Voronoi tesselation, whereas the SC scheme is based on the so-called "perfectly disordered" random microstructures [*Kröner*, 1978]. Since these two microstructures are different, their (exact) mechanical response may differ, and this may introduce a bias in the above comparisons. To evaluate this effect, we performed simulations similar to those presented above, but for the linear case, i.e., considering $n = 1$. In this case, the linearization is no longer needed and all extensions of the SC scheme reduce to the same SC estimate, so that the effect of the microstructure alone can be isolated. Results are not reported in detail here for the sake of conciseness, but we find that FFT and SC predictions provide very similar results, the discrepancy between them being less than 12% for $M = 1000$ with regard to the effective stress $\bar{\sigma}_{eq}/\tau_0$ and the overall heterogeneities $\Sigma(\sigma_{eq})/\bar{\sigma}_{eq}$ and $\Sigma(\dot{\varepsilon}_{eq})/\bar{\dot{\varepsilon}}_{eq}$. Note that for $M = 1000$ and $n = 1$, the overall heterogeneities reach values similar to those for $M = 70$ and $n = 3.5$, so that the local mechanical contrast of these two polycrystals can be compared. This result indicates that the discrepancies between the full-field and the various SC extensions tested are essentially attributable to the linearization procedure used in the mean-field approach.

[41] The TGT approach exhibits a response that departs significantly from the reference full-field results, for almost all results presented above. This model is therefore not well suited for olivine, the main drawback being that it allows the polycrystal to deform with only three independent slip systems, thus significantly underestimating the effective viscosity at large local anisotropy (large M). However, for certain aspects, it behaves qualitatively in a similar way to the Static bound, severely underestimating the stress heterogeneity associated with the intergranular interactions. This limitation was formulated in the original paper of *Lebensohn and Tomé* [1993] for highly nonlinear polycrystals (large n). The present results indicate that the same limitation holds also for low values of n, and large local anisotropy M. Attempts to artificially soften the intergranular interaction in this model by means of a scaling coefficient [e.g., see *Tommasi et al.*, 2000, equation (3)] makes the predictions even closer to the Static bound, which does not match the full-field solution either.

[42] The AFF extension shows much more reasonable predictions than the TGT estimate, especially in terms of predicting the stress and strain rate heterogeneities. Recall that solving the AFF equations does not require additional numerical cost compared to the TGT formulation. However, concerning the effective behavior, the AFF model predicts an overly rapid increase of $\bar{\sigma}_{eq}$ with the anisotropy parameter M, as compared to the full-field solution. For $M > 20$, it is even observed that the predicted effective stress is larger than that given by the VAR procedure which, it should be recalled, provides a rigourous bound for the effective potential $\tilde{U}$. Since it has been verified that the same feature is observed also for a rigorously isotropic polycrystal generated with many more crystal orientations than considered here, it can be concluded that the AFF extension violates the VAR bound for $M > 20$. This provides, from a theoretical point of view, a strong limit to the applicability of the AFF procedure. Bound violation for the AFF extension has also been reported for other polycrystalline [*Bornert and Ponte Castañeda*, 1998; *Bornert et al.*, 2001] and composite [*Masson et al.*, 2000; *Ponte Castañeda*, 2002b] materials.

[43] The two mean-field procedures that are based on variational principles, namely VAR and SO estimations, provide by far the best estimates of polycrystal behavior. This is a remarkable result. Indeed, in spite of the complicated shape of the stress and strain rate distributions occurring in an actual polycrystal, as presented in section 3, these approaches still accurately capture, both qualitatively and quantitatively, the main features of the field statistics. This success is attributed to the fact that the linearized compliances depend explicitly on the second moment of the stress [*Ponte Castañeda*, 1991, 2002b]. It is also worth mentioning that these procedures do not increase considerably the numerical cost when compared to the AFF estimate (generally by a factor of about 20), so that subsequent coupling with a large-scale convection model may still be tractable.

[44] When compared to the AFF and TGT model, the VAR estimate not only significantly improves the estimation of the effective behavior, but also gives excellent predictions for the stress and strain rate field statistics. However, it has been found to be slightly inferior to the SO estimate for similar numerical cost. The SO estimate provides best overall results, especially for the effective behavior. The accuracy of this procedure has already been shown by *Idiart et al.* [2006] and *Rekik et al.* [2006] in the context of composite materials. The same conclusion has been drawn by *Lebensohn et al.* [2004b] for cubic and hexagonal viscoplastic polycrystals, and more recently by *Lebensohn et al.* [2007] with some preliminary results for olivine. We have extended these results by showing that excellent estimates for olivine are obtained not only for the effective behavior, but also for the field statistics. It must also be recalled that, as already mentioned, the SO estimate used here is an approximation of the original formulation of *Ponte Castañeda* [2002a] (that requires the numerical differentiation of the estimated effective stress potential), motivated by a reduction of numerical cost. As shown by *Liu and Ponte Castañeda* [2004], the original formulation is slightly more accurate. Furthermore, some corrective terms should be added to the solution obtained for the NPLCP in order to consistently estimate the field statistics in the nonlinear polycrystal of interest [*Idiart and Ponte Castañeda*, 2007a, 2007b]. Here, however, even with these simplifications, the SO estimate provides very good agreement with the reference FFT solution. It thus makes an excellent model for the micromechanical modeling of olivine.

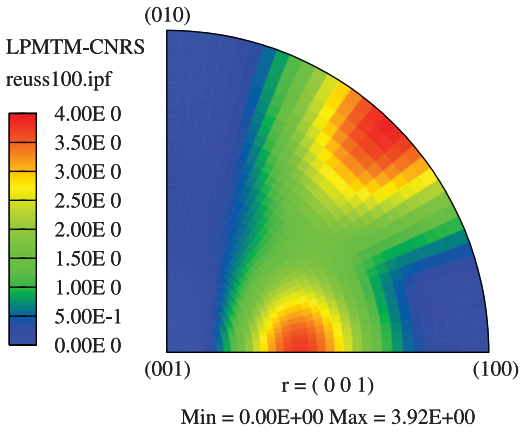

Figure 11. Inverse pole figures of the uniaxial compression axis showing the distribution of the normalized average equivalent strain rate $\dot{\varepsilon}_{eq}^{(r)}/\bar{\dot{\varepsilon}}_{eq}$ in crystal axes for the Static bound and $M = 100$.

[45] Concerning the VAR estimate, the exponent $k \simeq 0.5$ of the scaling law $\bar{\sigma}_{eq}/\tau_0 \propto M^k$ obtained for the effective behavior of olivine is compatible with the finding of *Nebozhyn et al.* [2000] in the context of hexagonal and ionic polycrystals, where k has been shown to be independent of the stress sensitivity n. This seems to indicate that the scaling exponent does not depend on the crystal structure, but only on the number of independent slip systems. Interestingly, the same exponent is also found here for the SO estimate, as reported recently by *Lebensohn et al.* [2007]. This seems to be a reasonable result since, beside matching the full-field results, $k \simeq 0.5$ is also the exponent given by the *linear* SC scheme, from which all nonlinear extensions derive.

[46] As already mentioned, besides the TGT model, the Static bound and the kinematic model of *Kaminski and Ribe* [2001] are often used to understand LPO development in the upper mantle. Several strong limitations of the Static model have already been discussed above, including the severe underestimation of the effective stress. This may be the reason why, using this model, *Dawson and Wenk* [2000] observed that the viscosity of polycrystalline olivine is far too low when inferred from single-crystal data. Figure 11 shows the distribution of $\dot{\varepsilon}_{eq}^{(r)}$ for the static model. Clearly, the strain rate does not show the correct distribution in the different crystal orientations. For example, it gives the highest values for crystals in orientations [101] and [110], whereas the reference solution predicts the highest value close to [111]. The kinematic model of *Kaminski and Ribe* [2001], which is an extension of *Ribe and Yu* [1991], does not account for intragranular stress and strain heterogeneities either. This model is based on a minimization of the overall difference between the strain rate of each grain and the macroscopic strain rate at the polycrystal level. Although the formulation has been proposed to deal with polycrystals with less than five independent slip systems, the same principle, if appropriate, should be applicable to more general cases, such as the polycrystal considered here comprising five independent systems. In that case, the solution of the minimization problem would be exactly the Taylor bound, which has been shown to depart in many ways from our reference results. We therefore anticipate that estimations of microstructure evolution inferred from the Static bound or from the kinematic model may not be physically sound. In other words, even if the correct mechanical and thermodynamical parameters are considered at the grain scale, the predicted mechanical state at grain and polycrystal levels may not be accurate.

6.2. Implications for Deformation Mechanisms

[47] The results obtained for the overall stress and strain rate heterogeneities suggest the following comments. First of all, the (suitably normalized) heterogeneities $\Sigma(\sigma_{eq})/\bar{\sigma}_{eq}$ and $\Sigma(\dot{\varepsilon}_{eq})/\bar{\dot{\varepsilon}}_{eq}$ obtained for olivine are significantly larger than those reported by *Lebensohn et al.* [2004b] for cubic (FCC) polycrystals, which have a value of about 0.5 for $n = 10$. This highlights the effect of the local anisotropy on the local mechanical state of the polycrystal since, even at high stress sensitivity, FCC grains exhibit a much smaller anisotropy than olivine. We have shown that in olivine, local equivalent stress and strain rate can be significantly larger than their macroscopic counterparts for large M values, as a result of the intergranular interactions. Furthermore, our results are also significantly larger than those obtained for ice polycrystals (which exhibit a stress exponent $n = 3$ similar to olivine), for which values smaller than 1.5 have been reported for $M = 100$ [*Lebensohn et al.*, 2004b]. In fact, even in the linear case ($n = 1$), it can be shown that both $\Sigma(\sigma_{eq})/\bar{\sigma}_{eq}$ and $\Sigma(\dot{\varepsilon}_{eq})/\bar{\dot{\varepsilon}}_{eq}$ increase more rapidly for olivine (both growing approximately as $M^{0.25}$) than for two examples of hexagonal materials, namely, ice (two independent slip systems) and zirconium (four independent systems), which exhibit saturation ($\propto M^0$). Since olivine has three independent systems, one may intuitively expect a similar behavior, but this is not actually the case. Such a feature could be associated with the geometry of the slip systems in olivine. In any case, the large increase of Σ values with M reflects a growing localization of the stress and strain rate in the polycrystal. We have seen in section 3.3 that localization bands become steadily thinner and more intense as M increases.

[48] In this study, we have considered a series of physically relevant slip systems besides the artificial $\{111\}\langle 1\bar{1}0\rangle$. However, it turns out that several of them have a very minor influence on olivine behavior, at least for the $\tau_{0(k)}$ values considered here. This is the case of the hard slip systems with Burger's vector aligned with the **a** or **c** lattice directions. Indeed, for $M = 10$, the three easiest slip systems (i.e., (010)[100], (001)[100], and (010)[001]) contribute as much as 92% to the total strain rate (SO estimation). For $M = 100$, their contribution is larger than 97%. All other secondary systems share the remaining part of the deformation. Among them, $\{111\}\langle 1\bar{1}0\rangle$, which somehow represents here the accommodation mechanisms in the real material, has a very minor contribution to the overall strain, but it is of primary importance for the micromechanical modeling: its strength completely determines the overall viscosity of olivine, this system providing the necessary additional independent systems. However, concerning the other secondary (hard) slip systems, namely (100)[001], {011}[100], {031}[100], and {110}[001], it was found a

posteriori that they were unimportant, since they affect only very weakly the effective viscosity, and their contribution to the overall deformation is really small when compared to the three softest systems.

[49] One of the issues remaining in the present work, and probably not a simple one, is the replacement of the system $\{111\}\langle 1\bar{1}0\rangle$ by a more realistic accommodation process, i.e., that has been observed in real specimens. Recall that, to the best of our knowledge, accommodation processes based on physical mechanisms (grain boundary sliding, diffusion, dislocation climb,...) have not yet been successfully implemented in micromechanical models. However, this will be necessary in order to obtain realistic estimation of the microstructure evolution (LPO, grain size,...) and the associated viscoplastic anisotropy within the upper mantle. First of all, it is worth noting that distinct accommodation processes may be active in laboratory versus under in situ conditions, owing to the huge difference in strain rates ($\sim$10 orders of magnitude). The interpretation of laboratory experiments does not rule out the possible role of grain boundary mechanisms [*Karato et al.*, 1986]. According to *Hirth and Kohlstedt* [2003], grain boundary sliding may occur for small grain sizes at conditions corresponding to the transition between diffusion and dislocation creep regimes. *Zhang et al.* [2000] further report the strong influence of dynamic recrystallization on the mechanical behavior. In addition to the standard effect on LPO development, recrystallization may reduce grain size and thus promote diffusion creep, which could act as an effective accommodation process. For comparison, grain boundary migration, associated to diffusion processes, has been shown to be efficient for the absorption of dislocations in polar ices [*Chapelle et al.*, 1998]. On the other hand, there is abundant experimental evidence for the occurrence of climb of edge dislocations which, among other implications, would allow the formation of tilt boundaries [*Goetze and Kohlstedt*, 1973]. *Durham and Goetze* [1977] and *Durham et al.* [1977] have shown the importance of considering climb in the interpretation of their mechanical tests on single crystals, and further estimate that this mechanism could contribute as much as 10–20% to the total deformation for some specific crystal orientations (a value that seems rather high). According to *Bai et al.* [1991] and *Bai and Kohlstedt* [1992], climb may be the rate-controlling mechanism for polycrystals, at least for certain specific experimental conditions, but this mechanism should lead to stress sensitivity higher than observed, $n \sim 5$ [*Weertman*, 1999]. Climb seems to be more active at high temperature [*Phakey et al.*, 1972] and may occur at higher rate under wet conditions [*Mackwell et al.*, 1985]. These latter authors also suggest that the weakening observed under wet conditions, as compared to dry conditions, is due to enhancement of the rate of climb of dislocations in the wet experiments. Finally, *Hirth and Kohlstedt* [2003] and *Mei and Kohlstedt* [2000] argue that climb is rate-limited by the pipe diffusion of Si, a mechanism that would lead to a stress sensitivity $n \sim 3.7$, i.e., compatible with single crystal and polycrystal data. In any case, it is not the aim of this paper to discuss whether creep is controlled by dislocation glide (dislocations move a long distance by glide in a slow and impeded manner and then quickly a short distance by climb) or dislocation climb (dislocations move unimpeded quickly a long distance by glide and then slowly a short distance by climb). For this task, theoretical micromechanical models are of no help, since local deformation mechanisms are *input* for these models. However, we want to stress that the resistance of the accommodation process, whatever it may be, almost entirely determines the flow stress (and thus the viscosity) of olivine aggregates. Its precise experimental characterization is thus crucial.

[50] The climb of edge dislocations with Burgers vector parallel to [100] or [001] produces axial strain along the crystal direction **a** and **c**, respectively. However, while the edge component of the dislocation climbs, the screw component has to cross-slip to maintain the integrity of the mix dislocation on the new glide plane. This renders the strain that can be accommodated by climb rather complex [*Hartley*, 2003]. However, in any case, since climb allows axial deformation of the crystal lattice along the **a** or **c** direction, it provides at least a fourth independent system. On the other hand, four systems are sufficient to deform olivine polycrystals. This can be demonstrated, as detailed by *Castelnau et al.* [2008], by adding in the FFT (or equivalently SO) model a new slip system allowing axial deformation along **a** and **c** directions (but not along **b**), and verifying that the effective stress $\bar{\sigma}_{eq}$ tends to a finite limit as $M \to \infty$. This last result is also consistent with the theoretical findings of *Nebozhyn et al.* [2000] and *Lebensohn et al.* [2007].

[51] Finally, for future work, one difficulty will be to assess the relative resistance of accommodation mechanisms since, again, they essentially determine the flow stress of olivine polycrystals. Since these mechanisms only contribute weakly to the overall deformation, as evidenced above, the experimental characterization of their mechanical response may be rather difficult.

6.3. LPO Development

[52] This study has been focused on the instantaneous behavior rather than microstructural evolution at large strain. However, it has been shown by *Liu et al.* [2003a, 2003b], and *Lebensohn et al.* [2007] that the VAR and SO estimates can also provide an improved description of LPO development in metallic alloys and in halite, when compared to the TGT model. The observed improvement is due to a more realistic distribution of stress and strain rate in the polycrystal, as also observed here for olivine. However, it is worth emphasizing that, within mean-field approaches, all the treatments proposed for microstructure evolution are based on the sole use of phase-average fields. Thus for example, LPO evolution is classically related to the mean shear-rate $\dot{\gamma}^{(r)}_{(k)}$. However, it has been shown that the local shear-rate $\dot{\gamma}(\mathbf{x})$ can differ significantly from its phase average, owing to the strong intergranular interactions occurring in olivine. The *local* rotation of the crystal lattice must occur in response to the local mechanical state and not to some average quantities. Neglecting the intragranular heterogeneities of strain rate leads to LPO predictions that are too pronounced at large strain, as has been reported in the literature. Similar limitations also apply to the prediction of dynamic recrystallization. In the model of *Wenk and Tomé* [1999], for example, the stored energy is directly related to the phase average value $\tau^{(r)}_{(k)}$. Recrystallization is however a local process depending heavily on local

energy gradients. It is therefore expected to be highly sensitive to the intra- and intergranular heterogeneities. Similar observations have been reported by *Castelnau et al.* [2006] in the context of strain hardening, which have shown that accounting for the intraphase heterogeneities allows a better match between the SC model and the full-field reference solution.

[53] Given that the SO model is capable of accurately reproducing certain features of the full-field solutions, including the distribution of intraphase stresses and strain rates, it is anticipated that subsequent developments (currently under investigation) should also lead to more accurate treatments of LPO evolution and dynamic recrystallization in olivine polycrystals.

7. Concluding Remarks

[54] In this study, reference solutions for the rheological behavior of olivine polycrystals have been generated by means of the full-field FFT method. This method provides the mechanical response of polycrystalline aggregates with grain shape and arrangement following a random Voronoi tesselation. The full-field results have been compared to several mean-field approaches, all of them obtained by a different nonlinear generalization of the Self-Consistent scheme for viscoplasticity. The slip systems considered at the grain scale, and their corresponding behavior, are appropriate for creep of dry olivine at high temperature and low pressure. For isotropic polycrystals, we find that the TGT model, generally denoted "VPSC" in the geophysical literature, provides results that differ significantly from the reference solutions. On the other hand, excellent agreement with the full-field solution has been obtained for the SO method, not only for the effective behavior, but also for the field statistics as a function of the crystal orientation. The success of the SO method (which also applies, though to a lesser degree, to the VAR method) can be attributed to a more refined linearization procedure accounting explicitly for the intraphase stress heterogeneities. The AFF estimate provides results that are not as good as SO and VAR methods, but that are, however, far better than TGT predictions, and at a comparable cost (to the latter).

[55] The computed stress and strain rate heterogeneities in deforming olivine have been found to be considerable, i.e., larger than for standard cubic and hexagonal materials. Furthermore, our results show that olivine cannot deform with only three independent slip systems, as had been previously suggested using the TGT model. However, we find that four systems are sufficient, in agreement with the theoretical predictions of *Nebozhyn et al.* [2000]. The necessary additional accommodation mode would be provided through grain boundary mechanisms or by dislocation climb as had often been reported in the literature. It is worth emphasizing that the overall strength of olivine polycrystals may thus be essentially determined by the resistance of this additional mode.

[56] To extend our results to peridotites under thermomechanical conditions relevant for the upper mantle, it would be necessary to deal with the effect of pyroxene, for which relatively scarce mechanical data have been published, but which is apparently stiffer than olivine while exhibiting only one easy slip system. Furthermore, the presence of liquid inclusions with very small or vanishing viscosity, may have a large effect on the overall viscosity, e.g., beneath an oceanic spreading center or under volcanic arcs in subduction zones. Given the relatively larger contrast in mechanical properties of peridotites, compared to the polycrystals of pure olivine considered in this work, it is expected that the SO model should give even larger improvements in accuracy for rheological behavior and texture development in these materials (over the standard texturing models).

[57] **Acknowledgments.** The authors are grateful to Pierre Gilormini (CNRS-ENSAM, France) and Nicolas Rupin (Ecole Polytechnique, France) for their initial help in the computation of the VAR estimate, and to Thorsten Becker (Univ. Southern Cal., USA) for his fruitful comments. We greatly appreciated the very interesting comments of J. Weertman on climb and glide mechanisms, and the constructive remarks of an anonymous reviewer. The sabbatical leave of O. Castelnau at IGPP was funded by CNRS and the Green Foundation at IGPP/SIO. The work of P. Ponte Castañeda was supported by NSF grant CMS-02-01454.

References

Bai, Q., and D. L. Kohlstedt (1992), High-temperature creep of olivine single crystals. Part II: Dislocation structures, *Tectonophysics*, *206*, 1–29.

Bai, Q., S. J. Mackwell, and D. L. Kohlstedt (1991), High-temperature creep of olivine single crystals: 1. Mechanical results for buffered samples, *J. Geophys. Res.*, *96*, 2441–2463.

Blackman, D. K. (2007), Use of mineral physics, with geodynamic modeling and seismology, to investigate flow in the earth's mantle, *Rep. Prog. Phys.*, *70*, 659–689.

Blackman, D. K., and J.-M. Kendall (1997), Sensitivity of teleseismic body waves to mineral texture and melt in the mantle beneath a mid-ocean ridge, *Philos. Trans. R. Soc., Ser. A*, *355*, 217–231.

Blackman, D. K., H. R. Wenk, and J. M. Kendall (2002), Seismic anisotropy of the upper mantle: 1. Factors that affect mineral texture and effective elastic properties, *Geochem. Geophys. Geosyst.*, *3*(9), 8601, doi:10.1029/2001GC000248.

Bobeth, M., and G. Diener (1987), Static and thermoelastic field fluctuations in multiphase composites, *J. Mech. Phys. Solids*, *35*, 137–149.

Bornert, M., and P. Ponte Castañeda (1998), Second-order estimates of the self-consistent type for viscoplastic polycrystals, *Proc. R. Soc., Ser. A and Ser. B*, *A454*, 3035–3045.

Bornert, M., R. Masson, P. Ponte Castañeda, and A. Zaoui (2001), Second-order estimates for the effective behaviour of viscoplastic polycrystalline materials, *J. Mech. Phys. Solids*, *49*, 2737–2764.

Braun, M. G., G. Hirth, and E. M. Parmentier (2000), The effect of deep damp melting on mantle flow and melt generation beneath mid-ocean ridges, *Earth Planet. Sci. Lett.*, *176*, 339–356.

Brenner, R., O. Castelnau, and L. Badea (2004), Mechanical field fluctuations in polycrystals estimated by homogenization techniques, *Proc. R. Soc., Ser. A and Ser. B*, *A460*(2052), 3589–3612.

Bresser, J. H. P. D., J. H. T. Heege, and C. J. Spiers (2001), Grain size reduction by dynamic recrystallization: Can it result in major rheological weakening?, *Int. J. Earth Sci.*, *90*, 28–45.

Castelnau, O., G. Canova, R. Lebensohn, and P. Duval (1997), Modelling viscoplastic behavior of anisotropic polycrystalline ice with a self-consistent approach, *Acta Mater.*, *45*, 4823–4834.

Castelnau, O., R. Brenner, and R. Lebensohn (2006), The effect of strain heterogeneity on the work-hardening of polycrystals predicted by mean-field approaches, *Acta Mater.*, *54*, 2745–2756.

Castelnau, O., R. A. Lebensohn, P. Ponte Castañeda, and D. K. Blackman (2008), Earth mantle rheology inferred from homogenization theories, in *Multi-Scale Modeling of Heterogeneous Materials*, edited by F. Darve and O. Cazacu, chap. 4, pp. 55–70, John Wiley and Sons.

Chapelle, S. D. L., O. Castelnau, V. Lipenkov, and P. Duval (1998), Dynamic recrystallization and texture development in ice as revealed by the study of deep ice cores in antarctica and greenland, *J. Geophys. Res.*, *103*, 5091–5105.

Chastel, Y. B., P. R. Dawson, H.-R. Wenk, and K. Bennett (1993), Anisotropic convection with implications for the upper mantle, *J. Geophys. Res.*, *98*, 17,757–17,772.

Christensen, U. R. (1987), Some geodynamical effects of anisotropy viscosity, *Geophys. J.*, *91*, 711–736.

Couvy, H., D. J. Frost, F. Heidelbach, K. Nyilas, T. Ungar, S. Mackwell, and P. Cordier (2004), Shear deformation experiments of forsterite at 11 gpa −1400c in the multianvil apparatus, *Eur. J. Mineral.*, *16*, 877–889.

Dawson, P. R., and H. R. Wenk (2000), Texturing of the upper mantle convection, *Philos. Mag. A.*, *80*, 573–598.

de Botton, G., and P. Ponte Castañeda (1995), Variational estimates for the creep behaviour of polycrystals, *Proc. R. Soc., Ser. A and Ser. B*, *A448*, 121–142.

Durham, W. B., and C. Goetze (1977), Plastic flow of oriented single crystals of olivine: 2. Mechanical data, *J. Geophys. Res.*, *82*(36), 5737–5753.

Durham, W. B., C. Goetze, and B. Blake (1977), Plastic flow of oriented single crystals of olivine: 2. Observations and interpretations of the dislocation structures, *J. Geophys. Res.*, *82*(36), 5755–5770.

Durinck, J., A. Legris, and P. Cordier (2005), Pressure sensitivity of olivine slip systems: First-principle calculations of generalized stacking faults, *Phys. Chem. Miner.*, *32*, 646–654.

Eshelby, J. D. (1957), The determination of the elastic field of an ellipsoidal inclusion, and related problems, *Proc. R. Soc., Ser. A and Ser. B*, *A241*, 376–396.

Gilormini, P. (1995), A critical evaluation for various nonlinear extensions of the self-consistent model, in *Proc. IUTAM Symp. on Micromechanics of Plasticity and Damage of Multiphase Materials*, edited by A. Pineau and A. Zaoui, pp. 67–74, Klower Acad. Publ., Sèvres, France.

Goetze, C., and D. L. Kohlstedt (1973), Laboratory study of dislocation climb and diffusion in olivine, *J. Geophys. Res.*, *78*, 5961–5971.

Hartley, C. (2003), A method for linking thermally activated dislocation mechanisms of yielding with continuum plasticity theory, *Philos. Mag. A and B*, *83*, 3783–3808.

Hershey, A. V. (1954), The elasticity of an isotropic aggregate of anisotropic cubic crystals, *J. Appl. Mech.*, *21*, 236–240.

Hirth, G., and D. Kohlstedt (2003), Rheology of the upper mantle and the wedge: A view from the experimentalists, *Geophys. Monogr.*, *138*, 83–105.

Hutchinson, J. W. (1977), Creep and plasticity of hexagonal polycrystals as related to single crystal slip, *Metall. Trans. A and B*, *8A*(9), 1465–1469.

Idiart, M., and P. Ponte Castañeda (2007a), Field statistics in nonlinear composites. part I: Theory, *Proc. R. Soc., Ser. A and Ser. B*, *463*, 183–202, doi:10.1098/rspa.2006.1756.

Idiart, M., and P. Ponte Castañeda (2007b), Field statistics in nonlinear composites. part II: Applications, *Proc. R. Soc., Ser. A and Ser. B*, *463*, 203–222, doi:10.1098/rspa.2006.1757.

Idiart, M. I., H. Moulinec, P. Ponte Castañeda, and P. Suquet (2006), Macroscopic behavior and field fluctuations in viscoplastic composites: Second-order estimates versus full-field simulations, *J. Mech. Phys. Solids*, *54*, 1029–1063.

Jung, H., and S. Karato (2001), Water-induced fabric transitions in olivine, *Science*, *293*, 1460–1463.

Kaminski, E., and N. M. Ribe (2001), A kinematic model for recrystallization and texture development in olivine polycrystal, *Earth Planet. Sci. Lett.*, *189*, 253–267.

Kaminski, E., N. M. Ribe, and J. T. Browaeys (2004), D-rex, a program for calculation of seismic anisotropy due to crystal lattice preferred orientation in the convective upper mantle, *Geophys. J. Int.*, *158*, 744–752.

Kanit, T., S. Forest, I. Galliet, V. Mounoury, and D. Jeulin (2003), Determination of the size of the representative volume element for random composites: Statistical and numerical approach, *Int. J. Solids Struct.*, *40*, 3647–3679.

Karato, S., and P. Wu (1993), Rheology of the upper mantle: A synthesis, *Science*, *260*, 771–778.

Karato, S., M. S. Paterson, and J. D. Fitzgerald (1986), Rheology of synthetic olivine aggregates: Influence of grain size and water, *J. Geophys. Res.*, *91*, 8151–8176.

Kocks, U. F., C. N. Tomé, and H. R. Wenk (1998), *Texture and Anisotropy*, Cambridge Univ. Press, New York.

Kohlstedt, D., and M. E. Zimmerman (1996), Rheology of partially molten mantle rocks, *Annu. Rev. Earth Planet. Sci.*, *24*, 41–62.

Kreher, W. (1990), Residual stresses and stored elastic energy of composites and polycrystals, *J. Mech. Phys. Solids*, *38*, 115–128.

Kröner, E. (1958), Berechnung der elastischen konstanten des vielkristalls aus den konstanten des einkristalls, *Z. Phys.*, *151*, 504–518.

Kröner, E. (1978), Self-consistent scheme and graded disorder in polycrystal elasticity, *J. Phys.*, *8*, 2261–2267.

Lebensohn, R. A. (2001), N-site modeling of a 3D viscoplastic polycrystal using fast Fourier transform, *Acta Mater.*, *49*, 2723–2737.

Lebensohn, R. A., and C. N. Tomé (1993), A self-consistent anisotropic approach for the simulation of plastic deformation and texture development of polycrystals: Application to zirconium alloys, *Acta Metall. Mater.*, *41*(9), 2611–2624.

Lebensohn, R. A., Y. Liu, and P. Ponte Castañeda (2004a), Macroscopic properties and field fluctuations in model power-law polycrystals: Full-field solutions versus self-consistent estimates, *Proc. R. Soc., Ser. A and Ser. B*, *A460*, 1381–1405.

Lebensohn, R. A., Y. Liu, and P. Ponte Castañeda (2004b), On the accuracy of the self-consistent approximation for polycrystals: Comparison with full-field numerical simulations, *Acta Mater.*, *52*, 5347–5361.

Lebensohn, R. A., C. N. Tomé, and P. Ponte Castañeda (2007), Self-consistent modeling of the mechanical behavior of viscoplastic polycrystals incorporating field fluctuations, *Philos. Mag. A and B*, *87*(28), 4287–4322.

Liu, Y., and P. Ponte Castañeda (2004), Second-order theory for the effective behavior and field fluctuations in viscoplastic polycrystals, *J. Mech. Phys. Solids*, *52*, 467–495.

Liu, Y., P. Gilormini, and P. Ponte Castañeda (2003a), Variational self-consistent estimates for texture evolution in viscoplastic polycrystals, *Acta Mater.*, *51*, 5425–5437.

Liu, Y., P. Gilormini, and P. Ponte Castañeda (2003b), Homogenization estimates for texture evolution in halite, *Tectonophysics*, *406*, 179–195.

Mackwell, S. J., D. L. Kohlstedt, and M. S. Paterson (1985), The role of water in the deformation of olivine single crystals, *J. Geophys. Res.*, *90*, 11,319–11,333.

Mainprice, D., A. Tommasi, H. Couvy, P. Cordier, and D. J. Frost (2005), Pressure sensitivity of olivine slip systems and seismic anisotropy of Earth's upper mantle, *Nature*, *433*, 731–733.

Mangeney, A., F. Califano, and K. Hutter (1997), A numerical study of anisotropic, low-reynolds number, free surface flow for ice sheet modeling, *J. Geophys. Res.*, *102*, 22,749–22,764.

Masson, R., M. Bornert, P. Suquet, and A. Zaoui (2000), An affine formulation for the prediction of the effective properties of nonlinear composites and polycrystals, *J. Mech. Phys. Solids*, *48*, 1203–1226.

Mei, S., and D. L. Kohlstedt (2000), Influence of water on plastic deformation of olivine aggregates: 2. Dislocation crrep regime, *J. Geophys. Res.*, *105*, 21,471–21,481.

Michel, J.-C., H. Moulinec, and P. Suquet (2000), A computational method based on augmented lagrangians and fast Fourier transforms for composites with high contrast, *Comput. Modell. Eng. Sci.*, *1*, 79–88.

Molinari, A., G. R. Canova, and S. Ahzi (1987), A self-consistent approach of the large deformation polycrystal viscoplasticity, *Acta Metall.*, *35*(12), 2983–2994.

Moulinec, H., and P. Suquet (1994), A fast numerical method for computing the linear and nonlinear mechanical properties of composites, *C. R. Acad. Sci. Paris*, *318*(IIb), 0417–1413.

Moulinec, H., and P. Suquet (1998), A numerical method for computing the overall response of nonlinear composites with complex microstructure, *Comput. Methods Appl. Mech. Eng.*, *157*, 69–94.

Nebozhyn, M. V., P. Gilormini, and P. Ponte Castañeda (2000), Variational self-consistent estimates for viscoplastic polycrystals with highly anisotropic grains, *C. R. Acad. Sci. Paris*, *328*(IIb), 11–17.

Nebozhyn, M. V., P. Gilormini, and P. Ponte Castañeda (2001), Variational self-consistent estimates for cubic viscoplastic polycrystals: The effects of grain anisotropy and shape, *J. Mech. Phys. Solids*, *49*, 313–340.

Parks, D. M., and S. Ahzi (1990), Polycrystalline plastic deformation and texture evolution for crystals lacking five independent slip systems, *J. Mech. Phys. Solids*, *38*, 701–724.

Phakey, P., G. Dollinger, and J. Christie (1972), Transmission electron microscopy of experimentally deformed olivine crystals, in *Flow and Fracture of Rocks*, *Geophys. Monogr.*, vol. 16, edited by H. C. Heard et al., pp. 117–138, AGU, Washington, D. C.

Ponte Castañeda, P. (1991), The effective mechanical properties of nonlinear isotropic composites, *J. Mech. Phys. Solids*, *39*, 45–71.

Ponte Castañeda, P. (1996), Exact second-order estimates for the effective mechanical properties of nonlinear composite materials, *J. Mech. Phys. Solids*, *44*, 827–862.

Ponte Castañeda, P. (2002a), Second-order homogenization estimates for nonlinear composites incorporating field fluctuations. part I: Theory, *J. Mech. Phys. Solids*, *50*, 737–757.

Ponte Castañeda, P. (2002b), Second-order homogenization estimates for nonlinear composites incorporating field fluctuations. part II: Applications, *J. Mech. Phys. Solids*, *50*, 759–782.

Ponte Castañeda, P., and P. Suquet (1998), Nonlinear composites, *Adv. Appl. Mech.*, *34*, 171–302.

Press, W., B. Flannery, S. Teukolsky, and W. Vetterling (1992), *Numerical Recipes in Fortran: The Art of Scientific Computing*, 2nd ed., Cambridge Univ. Press, New York.

Raterron, P., J. Chen, L. Li, D. Weidner, and P. Cordier (2007), Pressure-induced slip-system transition in forsterite: Single-crystal rheological properties at mantle pressure and temperature, *Am. Mineral.*, *92*, 1436–1445.

Rekik, A., F. Auslender, M. Bornert, and A. Zaoui (2006), Objective evaluation of linearization procedures in nonlinear homogenization: A methodology and some implications on the accuracy of micromechanical schemes, *Int. J. Solid Struct.*, *44*, 3468–3496.

Ribe, N. M., and Y. Yu (1991), A theory for plastic deformation and textural evolution of olivine polycrystals, *J. Geophys. Res.*, *B5*, 8325–8335.

Sarma, G. B., and P. R. Dawson (1996), Effects of interactions among crystals on the inhomogeneous deformation of polycrystals, *Acta Mater.*, *44*(5), 1937–1953.

Soppa, E., P. Doumalin, P. Binkele, T. Wiesendanger, M. Bornert, and S. Schmauder (2001), Experimental and numerical characterisation of in-plane deformation in two-phase materials, *Comput. Math. Sci.*, *21*, 261–275.

Suquet, P. (1995), Overall properties of nonlinear composites: A modified secant moduli theory and its link with ponte castañeda nonlinear variational procedure, *C. R. Acad. Sci. Paris*, *320*(IIb), 563–571.

Tommasi, A., B. Tikoff, and A. Vauchez (1999), Upper mantle tectonics: Three-dimensional deformation, olivine crystallographic fabrics and seismic properties, *Earth Planet. Sci. Lett.*, *168*, 173–186.

Tommasi, A., D. Mainprice, G. Canova, and Y. Chastel (2000), Viscoplastic self-consistent and equilibrium-based modeling of olivine lattice preferred orientations: Implications for the upper mantle seismic anisotropy, *J. Geophys. Res.*, *105*, 7893–7908.

Weertman, J. (1975), High temperature creep produced by dislocation motion, in *Rate Processes in Plastic Deformation of Materials*, edited by J. C. M. Li and A. K. Mukherjee, pp. 315–336, ASM, John E. Dorn Mem. Symp., Cleveland, Ohio.

Weertman, J. (1999), Microstructural mechanisms in creep, in *Mechanics and Materials: Fundamentals and Linkages*, edited by M. Meyers, M. W. Armstrong, and H. Kirchner, pp. 451–488, John Wiley, New York.

Wenk, H. R., and C. N. Tomé (1999), Modelling dynamic recrystallization of olivine aggragates deformed in simple shear, *J. Geophys. Res.*, *104*, 25,513–25,527.

Wenk, H. R., K. Bennett, G. R. Canova, and A. Molinari (1991), Modelling plastic deformation of peridotite with the self-consistent theory, *J. Geophys. Res.*, *96*, 8337–8349.

Willis, J. R. (1981), Variational and related methods for the overall properties of composites, *Adv. Appl. Mech.*, *21*, 2–78.

Zhang, S., and S. Karato (1995), Lattice prefered orientation of olivine aggragates deformed in simple shear, *Nature*, *375*, 774–777.

Zhang, S., S. Karato, F. Fitzgerald, U. H. Faul, and Y. Zhou (2000), Simple shear deformation of olivine aggregates, *Tectonophysics*, *316*, 133–152.

D. K. Blackman, Institution of Geophysics and Planetary Physics, Scripps Institution of Oceanography, University of California San Diego, 9500 Gilman Drive, La Jolla, CA 92093-0225, USA. (dblackman@ucsd.edu)

O. Castelnau, Laboratoire des Propriétés Mécaniques et Thermodynamiques des Matériaux, CNRS, Université Paris Nord, av. J.B. Clément, 93430 Villetaneuse, France. (oc@lpmtm.univ-paris13.fr)

R. A. Lebensohn, Materials Science and Technology Division, Los Alamos National Laboratory, MST8-MS 755-LANL, Los Alamos, NM 87545, USA. (lebenso@lanl.gov)

P. Ponte Castañeda, Department of Mechanical Engineering and Applied Mechanics, University of Pennsylvania, 220 S. 33rd Street, Philadelphia, PA 19104-6315, USA. (ponte@seas.upenn.edu)